THE CRUSTAL STRUCTURE OF WINONA BASIN AS DETERMINED BY DEEP SEISMIC SOUNDING

by

STEVEN LYNCH

B.Sc., University of Guelph, 1975

A THESIS SUBMITTED IN PARTIAL FULFILLMENT OF

THE REQUIREMENTS FOR THE DEGREE OF

MASTER OF SCIENCE

in

THE FACULTY OF GRADUATE STUDIES

(Department of Geophysics and Astronomy)

We accept this thesis as conforming

to the required standard

THE UNIVERSITY OF BRITISH COLUMBIA

June, 1977

In presenting this thesis in partial fulfilment of the requirements for an advanced degree at the University of British Columbia, I agree that the Library shall make it freely available for reference and study. I further agree that permission for extensive copying of this thesis for scholarly purposes may be granted by the Head of my Department or by his representatives. It is understood that copying or publication of this thesis for financial gain shall not be allowed without my written permission.

Department of Geophysics and Astronomy

The University of British Columbia
2075 Wesbrook Place
Vancouver, Canada
V6T 1W5

Date Sept 27 1977

ABSTRACT

During August 1975, three reversed deep seismic sounding profiles were run over Winona Basin, a deep water sedimentary basin located west of the northern end of Vancouver Island. This thesis reports on the analysis of the data for reversed profiles 75-1 and 75-1R, which were recorded to distances of greater than 90 km along the axis of the basin.

The seismic signals from explosive charges are detected by six individual hydrophones, amplified and recorded on a multi-channel digital acquisition system.

The sub-critical reflection data and the refraction data are amplitude corrected for spherical spreading, amplifier gain, charge size and varying hydrophone sensitivity. Immediately prior to compilation into record sections, the data are bandpass filtered to improve their general appearance.

Three methods of analysis were used to obtain velocity-depth information from the sub-critical reflection data; the ray parameter, T^2-X^2 and the stripped T^2-X^2 methods. A comparison of the results obtained from the three techniques shows that the ray parameter and T^2-X^2 methods yield essentially the same result, whereas the stripped T^2-X^2 method is of no use in analysing the data below the second sub-bottom layer. The analysis of profile 75-1R data at the northwest end of the basin gave a sedimentary structure divided into three

prominent horizons, with velocities ranging from 1.7 to 2.1 km/s. The total depth to the basaltic layer was determined to be 1.8 km. This thickness is considerably less than that suggested by other authors on the basis of gravity studies and assumptions concerning continuous seismic profiles. Due to the presence of significant dips on the reflecting horizons in the southeast, no velocity-depth information could be obtained from the analysis of profile 75-1.

Calculation of a preliminary velocity-depth model based on first arrival travel times was the first step in the analysis of the refraction data. These iso-velocity layered models provided an initial interpretive guide and a starting place for the calculation of synthetic seismograms. In order to utilize traveltimes of first and secondary arrivals and the relative amplitude characteristics of the seismograms, the final interpretation made use of synthetic seismogram sections for comparison with the real data.

Based on such an analysis, the refraction data indicate that the crust underlying Winona Basin is separated into four sub-sediment layers, having significant velocity gradients. Average velocities and thicknesses for the layers are; 4.28 km/s, 1.6 km; 5.26 km/s, 2.75 km; 6.28 km/s, 4.13 km; 7.04 km/s, 3.76 km. The total sub-sediment thickness of this crustal section is thus 12 km. An unreversed mantle velocity of 7.8 km/s was interpreted from 75-1 results. On the basis of the velocity values, the layers have been identified with oceanic crustal layers 2a, 2b, 3a, 3b.

The thick crust is postulated to be the result of complex plate interactions occurring in the region. A comparison of the data from this work with previous studies in the region of Explorer and Juan de Fuca Ridges has led to the speculative conclusion that Winona Basin has been created within the last 3 to 4 my, by the slow northward progression of the Pacific-North America-Explorer plate triple point.

TABLE OF CONTENTS

LIST OF TABLES

List of Figures

ACKNOWLEDGEMENTS

For his encouragement, patience and support during the entirety of this project, I wish to express my deepest appreciation to Dr. R.M. Clowes. I am also indebted to W.B. Cumming who provided me with great assistance during the more technical aspects of the work.

This project has been aided greatly by the excellent quality of the data, due in no small way to the efforts of Dr. Bo Chandra, Chris West and Bill Cumming on the receiving ship, and George Spence, Patrick Shore and Rob Clayton on the shooting ship. Their diligence, enthusiasm and dedication are gratefully acknowledged.

Further, I wish to express my appreciation to the officers and crew of the C.F.A.V. ENDEAVOUR and C.F.A.V. LAYMORE for their assistance during the cruise. The assistance given by the explosives experts from the Fleet Diving Unit, Pacific Maritime Command is also gratefully acknowledged. The anti-submarine projectiles were supplied by the Seismology Division of the Earth Physics Branch.

Funding for this project was supplied by the National Research Council of Canada, operating grant A 7707. Additional funds were supplied by Mobil Oil Canada Ltd., Shell Canada Resources Ltd. and Chevron Standard. The Department of Energy Mines and Resources (Geological Survey of Canada) provided the contract to acquire the data and a research agreement to assist in its analysis.

1 INTRODUCTION

The tectonic structure west of Vancouver Island is, to say the least, extremely complicated. This region is the area of interaction between two major plates, the Pacific and North American, and two minor plates, the Explorer and Juan de Fuca plate (Fig 1.1). These smaller plates are the remnant of a much larger and ancient plate, the Farallon plate, which according to Atwater (1970) has been consumed by the overriding North American plate. Of special interest to this study is the location of the triple point between the three plates. It is thought to be somewhere near the region of 51° N 131° W; however, its absolute position is questionable. Winona Basin, the area of interest for this study, is located near the region of this triple point and is surrounded by the Pacific, North American and Explorer plates. What its role is, and how it is related to the complex plate tectonics, provided much of the impetus for the marine deep seismic sounding survey which was carried out in 1975.

1.1 Area of Study

The name Winona Basin was first applied to the deep sedimentary basin located at the foot of the continental margin off the northwest tip of Vancouver Island, by Srivastava et al (1971). The southernmost boundary is taken to be at the Brooks fracture zone, an area of intense fracturing and uplift, whereas the northern boundary is taken to be some

150 km to the northwest at the Dellwood Knolls. The basin is bounded on the west by Paul Revere Ridge and on the east by the edge of the continental slope. Fig 1.2 is a bathymetric map of the area detailing the major topographic features of the basin. The only major feature located within the interior of the basin itself is a broad low-relief structure named Winona Ridge. This feature trends somewhat obliquely to Paul Revere Ridge and is underlain by the stratified sediments of the basin. Other than this feature, the interior of the basin is flat lying with a mean water depth of approximately 2000 m.

A gravity survey over the area by Couch (1969) has revealed a -160 mgal free air anomaly located between Winona Ridge and the continental shelf. He interpreted this as being due to 4 to 6 km of sediments in this portion of the basin. This depth is consistent with later work by Tiffin et al (1973), who suggests that "the basin is underlain by approximately 4 km of mudstone, sandstone, conglomerate and minor coal of definite Pliocene-Pleistocene age".

On the basis of his gravity data, Couch (1969) generated a crustal and sub-crustal cross section along a line running from 48° N, 134° W to 52° N, 126° W. This section crosses Winona Basin at an oblique angle at roughly the midpoint of the basin and shows an approximate depth to the mantle of 15 km sub-bottom.

The basin is thought to be a relatively young structure, probably of Pliocene-Pleistocene age. This proposal has been given by Tiffin et al (1972) on the basis of limited

Fig 1.1

Location of Winona Basin with respect to the Pacific, North American, Explorer and Juan de Fuca plates. The area within the rectangle is shown enlarged on Fig 1.2. PA P, Pacific plate; AM P, North American plate; EX P, Explorer plate; JF P, Juan de Fuca plate. The hatchured line shows the assumed convergent boundary between Explorer/Juan de Fuca plates and the North American plate.

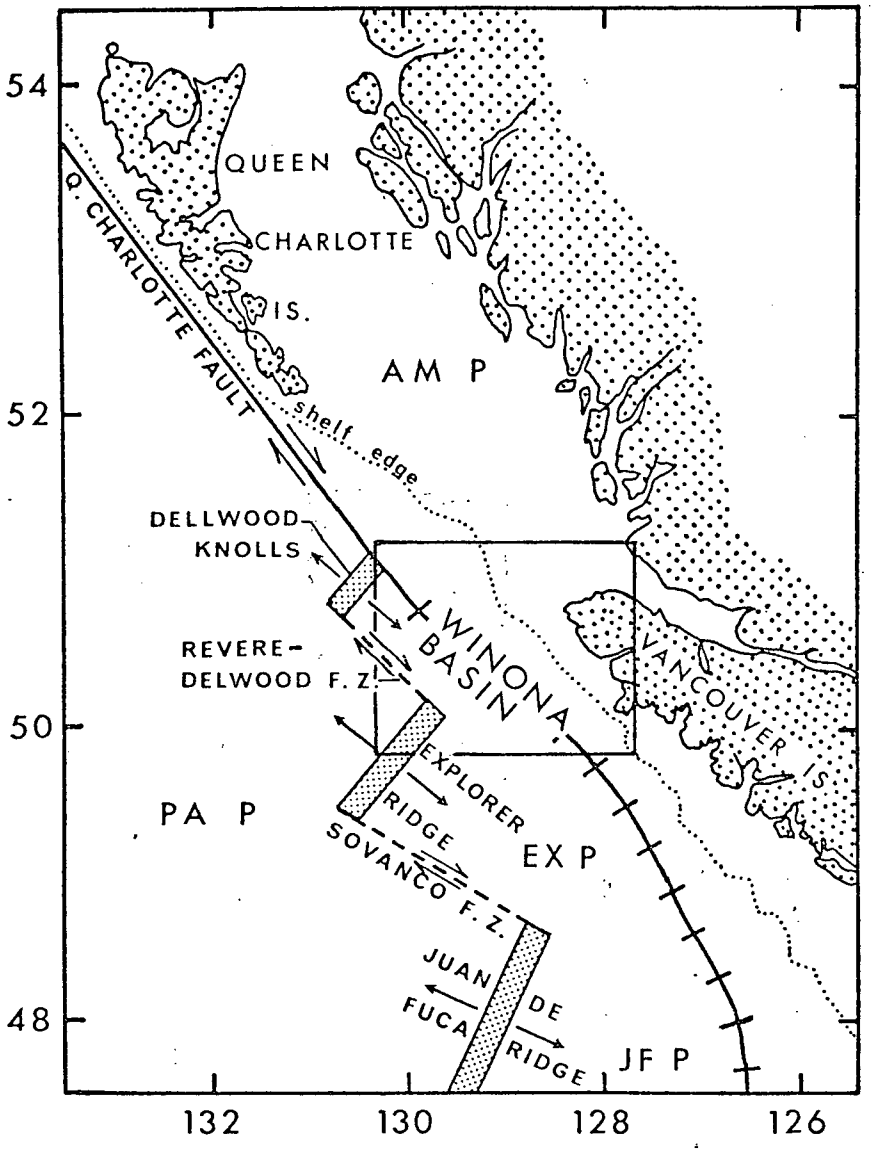
54
52
50
48
132
130
128
126
QUEEN
CHARLOTTE
IS.
Q. CHARLOTTE FAULT
shelf edge
AM P
DELLWOOD
KNOLLS
REVERE-
DELWOOD F. Z.
WINONA
BASIN
VANCOUVER IS.
EXPLORER
RIDGE
PA P
EX P
SOVANCO F. Z.
JUAN DE
FUCA RIDGE
JF P

Fig 1.2

Location of 1975 marine deep seismic sounding profiles in Winona Basin. Open circles show the drift track of the receiving ship during the profile run; heavy lines show the track of the shooting ship. Profiles 75-1 and 75-1R along the basin are the subject of this study. Bathymetric contours in meters (from Tiffin and Seemen, 1975).

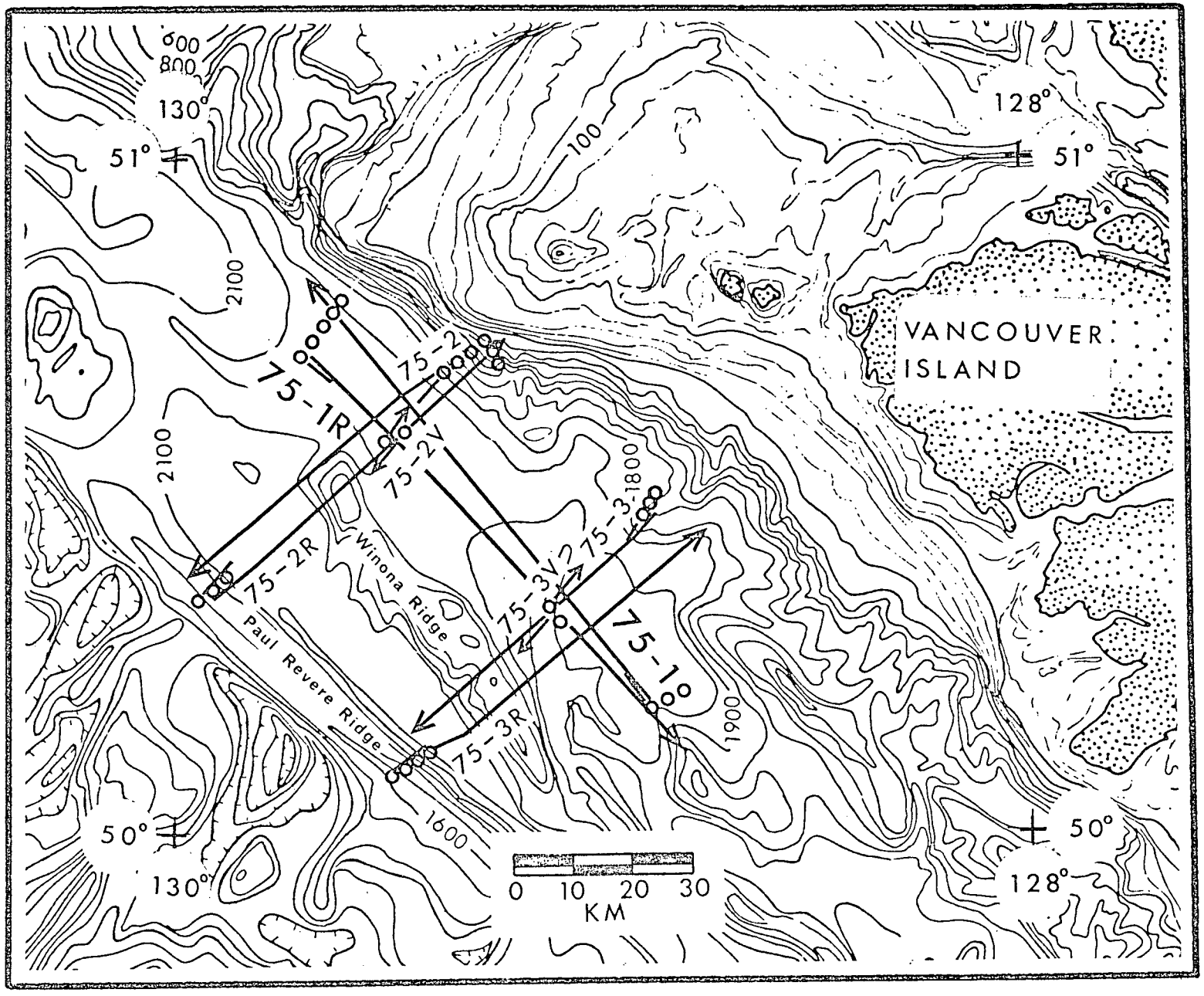
600
800
130°
51°
2100
2100
100
128°
51°
VANCOUVER
ISLAND
75-1R
75-2
75-2V
75-2R
Winona Ridge
75-3V2
75-3
1800
75-3V
75-1o
Paul Revere Ridge
75-3R
1900
1600
50°
130°
0 10 20 30
KM
50°
128°

formaniferal evidence.

The sediments in the basin are relatively undeformed in the northwest, as shown by Figs 1.3 and 1.4 (pocket on the rear cover); however, they are severely folded and faulted in the southeast, with the faults trending northwest (see Fig 1.5). Continuous seismic profile (C.S.P.) line 75-2 (Fig 1.4), shows the oceanic basement dipping eastward from Paul-Revere Ridge. It then dips beneath Winona ridge and can not be identified further on the profile.

Epicentral locations for earthquakes in the region have suggested the possibility that active deformation is presently taking place in the basin (Tobin and Sykes 1968). Milne et al (1977), however,have recently pointed out that there is a systematic bias in epicentral locations for the earthquakes off Canada's west coast. On the basis of this work and research currently in progress it appears likely that the majority of earthquakes are located on the Explorer Ridge/Revere-Dellwood fracture zone and not in the basin itself.

The area of Winona Basin was part of the original magnetic survey by Raff and Mason (1961) which provided much of the evidence for the introduction of the sea-floor spreading concept. In Winona Basin however, the anomalies show none of the magnetic lineations normally associated with a spreading centre, the magnetic structure of the basin being relatively smooth. There are normal magnetic lineations to the west in the region of Explorer Ridge; however, they terminate

Fig 1.3

A. Continuous seismic profile line 75-1, parallel to DSS profile 75-1. Penetration is achieved only to a maximum of 4 s two-way travel time.

B. Interpretation of C.S.P. line 75-1, courtesy of Hopkins (1976). Note the continuity along the profile of the interpreted reflecting horizons (located in pocket on the back cover).

Fig 1.4

A. Continuous seismic profile line 75-2 paralleling DSS profile 75-2. Note the relatively undeformed upper sediments, and the increase in fold amplitude with depth.

B. Interpretation of C.S.P. line 75-2, also from Hopkins (1976). On the lower right corner, basement has been interpreted as dipping to the east (also in pocket on back cover).

Fig 1.5

An air gun seismic profile over the deep water portion of Winona Basin beyond the base of the continental slope showing a thick folded and faulted sedimentary sequence, f=fault. Area between the arrows indicates the approximate position of reflection profile 75-1. Taken from Murray and Tiffin (1974).

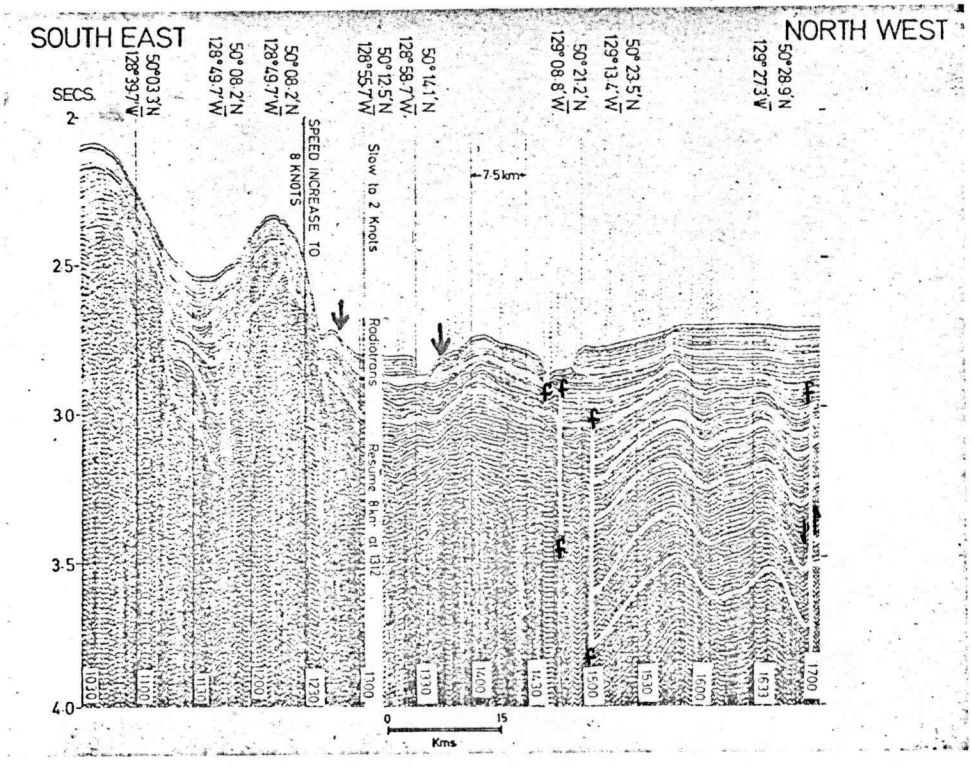
SOUTH EAST
NORTH WEST
SECS.
2
2·5
3·0
3·5
4·0
50°03·3'N
128°39·7'W
50°08·2'N
128°49·7'W
50°08·2'N
128°49·7'W
SPEED INCREASE TO
8 KNOTS
50°12·5'N
128°55·7'W
Slow to 2 Knots
50°14·1'N
128°58·7'W
7·5km
50°21·2'N
129°08·8'W
50°23·5'N
129°13·4'W
50°28·9'N
129°27·3'W
Radiotrans
Resume Run at 1312
1100
1130
1200
1230
1300
1330
1400
1430
1500
1530
1600
1630
1700
0
15
Kms

formaniferal evidence.

The sediments in the basin are relatively undeformed in the northwest, as shown by Figs 1.3 and 1.4 (pocket on the rear cover); however, they are severely folded and faulted in the southeast, with the faults trending northwest (see Fig 1.5). Continuous seismic profile (C.S.P.) line 75-2 (Fig 1.4), shows the oceanic basement dipping eastward from Paul-Revere Ridge. It then dips beneath Winona ridge and can not be identified further on the profile.

Epicentral locations for earthquakes in the region have suggested the possibility that active deformation is presently taking place in the basin (Tobin and Sykes 1968). Milne et al (1977), however, have recently pointed out that there is a systematic bias in epicentral locations for the earthquakes off Canada's west coast. On the basis of this work and research currently in progress it appears likely that the majority of earthquakes are located on the Explorer Ridge/Revere-Dellwood fracture zone and not in the basin itself.

The area of Winona Basin was part of the original magnetic survey by Raff and Mason (1961) which provided much of the evidence for the introduction of the sea-floor spreading concept. In Winona Basin however, the anomalies show none of the magnetic lineations normally associated with a spreading centre, the magnetic structure of the basin being relatively smooth. There are normal magnetic lineations to the west in the region of Explorer Ridge; however, they terminate

at Paul Revere Ridge and do not penetrate the basin itself.

1.2 Tectonic Significance of Winona Basin

The position of the triple point between the Pacific-North American and Explorer plates has been a source of conjecture for some time. Early work by Srivastava et al (1971) and Bertrand (1972) have suggested that the Dellwood Knolls, the northern boundary of Winona Basin, marks the present location of the triple point. Chase (1975) on the other hand has suggested that the triple point does not exist as a discrete point but rather it exists as a broad area of deformation.

Basing their conclusions on the lack of deformation of the shelf sediments north of Brooks fracture zone as opposed to the extreme deformation of the shelf sediments to the south of the fracture zone, Murray and Tiffin (1974) have proposed that the triple point was stable at the Brooks fracture zone until approximately 4 mya. This divides the continental margin off northern Vancouver Island into two different regimes: subduction, uplift and deformation to the south of Brooks fracture zone, and strike-slip motion to the north. They have suggested, however, that the triple point has migrated north in the last 4 my, resulting in the formation of the Winona Basin by the moving triple point. This would require the crust underlying the basin to be less than 4 my old.

Such a suggestion is supported by recent work of Riddihough (1977). From a detailed re-examination of the

existing magnetic anomaly patterns, he has calculated the Explorer-Juan de Fuca plate motions for the past 10 my. His results show that the triple point remained remarkably stable near the Brooks fracture zone until about 2 to 3 mya whereupon it started a slow northward miqration.

It is possible then that Winona Basin has been created very recently by the slow northward progression of the Pacific-North American-Explorer (P-A-E) plate triple point.

Another matter of debate is the position of the Pacific-North America plate boundary south of 51° N. North of 51° the boundary is defined by the Queen Charlotte transform fault zone. To the south, however, its location is less well established. If indeed the Dellwood Knolls do form the position of the P-A-E triple point, then south of 51° the Pacific and American plates are separated by Winona Basin. This idea requires that Winona Basin be part of the Explorer plate, or at least that it be independent of the American plate.

Barr and Chase (1974) suggested that the Pacific-American plate boundary now lies along a line connecting the northern edge of Juan de Fuca Ridge with the Queen Charlotte fault in the region of 51° N, 131° W. This was suggested on the basis of the available earthquake data and requires that the fault extend through Winona Basin. This would essentially isolate Explorer Ridge and thus render it inactive. However, recent ocean bottom seismometer results (G.C. Rogers, personal communication, 1977) have established the presence of seismic

activity on the northern branch of Explorer Ridge. This, plus the high heat flow values detected in the region by Srivastava et al (1971), and the fresh basalt dredged by Bertrand (1972) in the region of Explorer Ridge, make the conclusion of inactivity of the ridge unacceptable. In addition to this, a recent re-examination of the earthquake data for the area (Milne et al 1977) has shown serious systematic biases in the data with the result that most of the earthquakes are now believed to follow the Revere-Dellwood fracture zone system. It is unlikely then that the Queen Charlotte Fault extends through Winona Basin to the Juan de Fuca Ridge.

The recent relocation of the earthquake data for the area supports the idea of Chase et al (1975) that the Revere-Dellwood fracture zone is a transform fault. Unfortunately this does not clarify the position of Winona Basin to any great extent. The basin could be an isolated section of old Pacific plate material, an integral part of the North American plate or a recently formed addition to the Explorer-Juan de Fuca plate.

In any event, in order to completely understand the role Winona Basin plays in the complex tectonics of this region, additional geological and geophysical data are required. It was with this purpose in mind that a deep seismic sounding survey was run over the area of Winona Basin during the summer of 1975.

1.3 Data Acquisition and Profile Description

Project Description :

The main objective of this project is to supply detailed velocity and structural information for the crust and upper mantle beneath Winona Basin, in order that its role in the local tectonics may be further understood. To this end three reversed deep seismic sounding (DSS) profiles were run over the basin, their locations being shown on Fig 1.2. The deep seismic sounding method (Clowes, 1977), enables the recording of sub-critical reflections, wide angle reflections and refraction arrivals, with penetration being achieved from the ocean bottom to the upper mantle. As a method of delineating the shallow sedimentary structure of the basin, short sub-critical incidence reflection profiles with the shots at 7 m depth were recorded parallel to the start of each complete DSS profile and at the points of intersection of the cross profiles with profiles 75-1 and 75-1R. It was hoped that by placing the shots at this shallow depth they would blow out and minimise the bubble pulse problem. To delineate the deep sedimentary structure and possibly obtain sub-basement reflections, more energy was needed than could be obtained by placing the shots at 7 m. As a result, sub-critical incidence profiles were run using the source at 45 m depth. These profiles comprised the start of each DSS profile, thus enabling the interpreter to trace the transition from

reflection to refraction arrivals.

Continuous seismic profiles were also run along the length of each of the three reversed refraction lines. A 300 cu in air gun was used as the source with the recordings being on standard electrostatic paper. These profiles subsequently were analysed by Hopkins (1976).

Data Acquisition :

The method of data acquisition for the deep seismic sounding project is similar in principle to the two ship refraction technique described by Shor (1963). Operations at sea require one ship, in this case C.F.A.V. Endeavour, to drift freely and act as the recording ship while the second vessel, C.F.A.V. Laymore, proceeds along a predetermined path releasing the explosives. Detailed descriptions of the shooting procedures and data acquisition system are provided by Malecek (1976) and Clowes (1977). For this reason only a brief description of the methods and system will be given here.

Two types of shooting procedures were used during the profiles. Geogel, a commercial explosive, was used as the explosive source for the reflection profiles and out to a distance of 70 km on the refraction profiles. The charges ranged in size from 2.3 kg (5 lb) to 96 kg (200 lbs) and were suspended in the water by twine attached to large red party balloons. Detonation was accomplished by use of a timed fuse/Seismocap assembly and Primacord. For these shots, the

shot-to-ship distance was measured by use of a rangefinder focussed on the party balloons.

Beyond 70 km the explosive source consisted of three Mark IV H.E. anti-submarine projectiles per shot. Each projectile contained the equivalent of 94 kg of Minol high explosive, resulting in an equivilent charge size of 282 kg per shot. Due to their 68 kg casings the projectiles were far too heavy to be suspended by the party balloons. As an alternative, they were suspended from a raft made of empty 45 gallon drums. Detonation was similar to that used for the commercial explosives with the exception that the bombs were primed with plastic explosive. As a safety precaution, the bombs were detonated at distances in excess of 1 km from the shooting ship. As a result, the shot-to-ship distance had to be determined by the ship's radar.

The ship-to-ship distances were determined by radar out to a distance of approximately 22 km. Beyond this, LORAN A fixes had to be used to determine the ship's relative positions.

The direct water wave (D.W.W.) was detected at the shooting ship by means of a hydrophone trailed immediately behind the ship, and by a geophone located on the ship's deck. The two signals were recorded simultaneously with the WWVB time code on a 4 channel FM tape transport. The hydrophone and WWVB signals were recorded directly on a 2-channel Brush chart recorder played at a speed of 125 mm/s. These recordings were used to time the D.W.W. and the data recorded on tape was used

as a backup.

The receiving ship trailed a 610 m cable from which, at intervals of 91 m, 6 individual hydrophone systems and battery boxes were suspended to a depth of 45 m. The battery box was de-coupled from the main cable and hence surface wave action by shock cord. In order to provide additional mechanical damping, the hydrophone and a 15 m cable leading to the battery box were made neutrally bouyant by attaching flotation material.

The signal output from the hydrophone element is pre-amplified by 20 db and transmitted to amplifiers in the ship's laboratory. They are filtered using limits of 0.8 to 100 hz and then amplified by individual fixed gain amplifiers, manually set for each shot. The six analog signals plus WWVB time code are digitized on board the receiving ship at a frequency of 312.5 hz and then written onto magnetic tape using an I.B.M. compatible, 14 bit, multi-channel data acquisition system (Clowes 1977). Five of the six data channels plus the WWVB time code are monitored on a six-channel chart-recorder to ensure good quality control of the data.

Unfortunately, neither the recording ship nor the shooting ship had operational depth sounding equipment, although this was supposed to be available. Thus no record of the sea floor topography was obtained during the cruise.

2 PRELIMINARY ANALYSIS

2.1 Demultiplexing

As discussed in Section 1.4, the seven channel data set used in this study were recorded in multiplexed form on two digital field tapes. A sampling rate of 312.5 hz was used to digitize the analog signals on board the ship. Thus the sampling interval of the data is .0032 s and the Nyquist frequency is 156 hz. This high sampling rate was chosen to eliminate any aliasing problems associated with the high-cut filter (100 hz with a 12db/octave rolloff) of the analog amplifiers.

Far more data were stored on the field tapes than was actually needed. For this reason the data were demultiplexed and edited simultaneously as a preliminary step to the analysis. Approximately three seconds of data were kept before the first arrival for both reflection and refraction data. The termination for the reflection data was chosen to be immediately after the end of the second water bottom reflection whereas the cutoff for the refraction data was chosen to be immediately after the arrival of the direct water wave and super-critical water bottom reflections.

A number of problems were encountered during the demultiplexing of the data. During the process of digitizing and writing the analog signals from the hydrophones onto tape, the digitizer occaisionally "lost" data. Clowes (1977) has

described how such errors can occur with the marine data acquisition system. Also on a number of occasions the ship board operators failed to write "End of Files" at the termination of the data, resulting in the concatenation of several data files. At the time this study was begun, no demultiplexing program that would identify and correct these errors was available in the department. As a result, considerable effort was expended in writing a program that would handle all the errors associated with the field data. This program is now available for general use.

2.2 Origin Times

In all seismic work accurate determination of the time between the original seismic impulse, in our case the explosive detonation, and the arrival of the signal at a certain distance is of primary importance. As a result of the field technique used, the major source of error in the traveltime calculations is that associated with determining the origin time of the original seismic impulse. Since the explosive charges are detonated at depth, remote from the ship and by a timed fuse/Seismocap assembly, it is impossible to know the exact instant of detonation. Thus we must use the known distance and depth of the shot plus the known time of arrival of the explosive impulse at the hydrophone trailed behind the ship to extrapolate back to the origin time of the shot.

The paper chart recordings described in section 1.3 were

the only data set used to time the direct arrivals. Sufficient accuracy was obtained using these recordings and hence the back-up data on the FM tapes was never used. The arrival of the signal at the hydrophone could be timed to better than 5 ms from these chart recordings. The method of measuring the ship to shot distance has been described in section 1.3. The error in the rangefinder method is estimated to be less than 15%, which translates to an error of 15 m for the near shots (100 m) and 45 m for the farthest shots (300 m) in which this method was used. Using a water velocity of 1.49 km/s, these distance errors translate to timing errors of 10 ms and 30 ms, respectively.

The radar method of determining the distances to the anti-submarine projectiles was completely unreliable. The 45 gallon drums were so weighted down by the projectiles that they barely showed above the surface of the water. This made them very poor reflectors and thus the radar ranges obtained were useless. On subsequent cruises a radar reflector should be placed on the drums.

I was able, however, to devise an alternate method of obtaining the distances to these shots. Consider the following diagram :

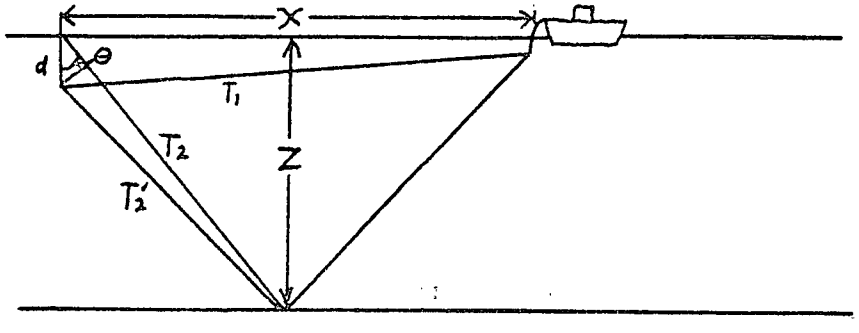

The method requires only a knowledge of the travel time difference between the direct arrival and the bottom bounce, plus the water depth to make it applicable to our data. The times of arrival of the direct wave T_1 and the bottom bounce T_2' are recorded and hence $T_2' - T_1$ is determined without knowing the actual length of either T_2' or T_1. In essence, the shot at depth D could be moved to the surface for the bottom reflection by applying the correction $Tc = D*\cos\theta/1.49$, where typically $\cos\theta = 0.97$. Then if we assume that the surface-to-surface travel path T_2 is the same as the T_2' travel path we have the following :

$$T_1 = (x^2 + d^2)^{1/2} / 1.49 \qquad 2.2\text{-}1$$

$$T_2 = (x^2 + 4z^2)^{1/2} / 1.49 \qquad 2.2\text{-}2$$

$$T_2 - T_1 = \{(x^2 + 4z^2)^{1/2} - (x^2 + d^2)^{1/2}\} / 1.49 \qquad 2.2\text{-}3$$

By assuming a reasonable value for the depth Z, we can use 2.2-3 by trial and error to find the value of X yielding the correct value of $T_2 - T_1$.

It is possible to perform the same type of analysis as above using the first and second bottom reflections. Such a method would yield X independently of the depth Z. However I was not able to time accurately the second bottom bounce and hence could not apply this procedure.

The error in the $T_2 - T_1$ method is estimated to be ± 100 m or correspondingly ± 66 ms using a 1.49 km/s water velocity; the main source of error is the lack of an adequately defined water depth. It is highly recommended that future cruises have working depth sounding equipment as the lack of adequate depth

knowledge was a hindrance not only in these calculations but in several other places throughout the study.

Corrections to obtain the true origin time of the shot were calculated using 2.2-1. The resulting corrections ranged from 70 ±15 ms for the near shots using the balloons to 250 ±35 ms for the farthest shots using balloons, and 1000 ±70 ms for the shots using the anti-submarine projectiles.

2.3 Shot-Receiver Distances

Once the origin time of the shot has been determined, the distance of the individual hydrophones from each shot must be calculated. This is done by timing the arrival of the direct water wave (D.W.W.) from the shot at the various hydrophones. From a knowledge of this arrival time, the origin time of the shot, and assuming a constant water velocity (1.49 km/s), the shot-receiver distances can be calculated. In so doing, it is assumed that the differences in the shot and receiver depths are insignificant.

The demultiplexed records of each shot were plotted at a density of 100 points/in (i.e. 1s=3.125 in) each point being one digitized value. The six seismic channels and W.W.V.B. were plotted simultaneously, each trace being normalised to a maximum amplitude of 0.75 in. The four seismograms shown on Fig 2.1 are typical of these records.

The direct water wave was then identified and the phase onset was timed with respect to the nearest second by using a millimeter ruler. Timing of first breaks for all clear D.W.W.

Fig 2.1

Four seismograms from profile 75-1, typical of those used to time the direct water wave and the first refraction arrivals. Approximate shot-receiver distances are; A) 0.5 km, B) 9.5 km, C) 94 km, D) 44 km. The upper trace of each seismogram is the WWVB time code. In (A), the direct arrival is overloading the hydrophone/amplifier combination.

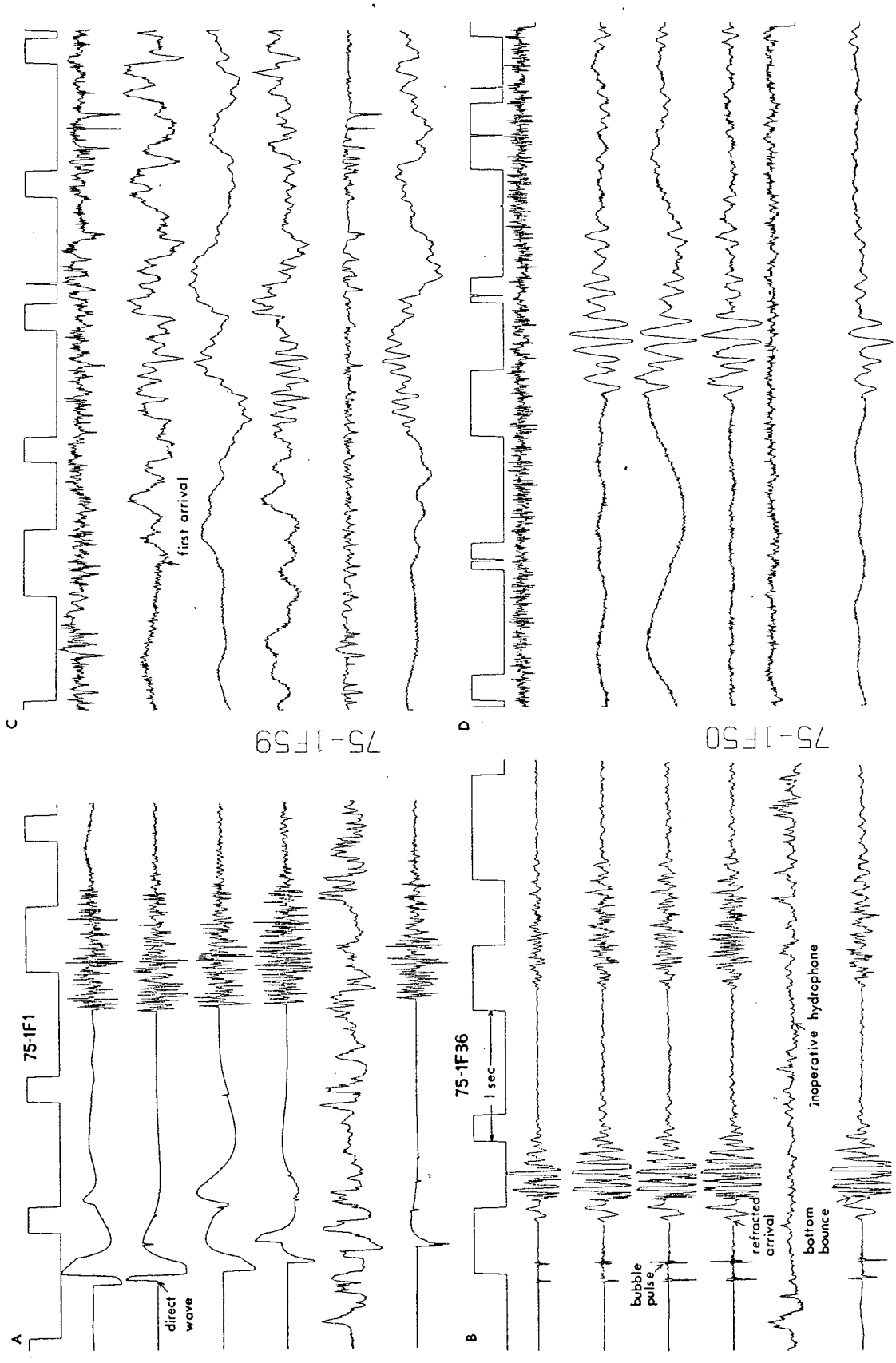
A
75-1F1
direct wave
B
75-1F36
1 sec
bubble pulse
refracted arrival
bottom bounce
inoperative hydrophone
C
first arrival
75-1F59
D
75-1F50

arrivals was better than 0.5 mm, corresponding to better than 7ms in time. Naturally not all shot-receiver distances could be calculated this simply. At distances greater than two kilometers along the reflection profiles using shots at 7 m depth, the direct wave became indistinct compared to the bottom bounce. This was probably due to the energy from the shots being trapped near the surface of the water and the hydrophones being too deep to detect it. This problem was not observed on the reflection profiles using shots at 45 m depth, i.e. with the shots the same depth as the hydrophones. In any case this was not catastrophic, the solution simply being to normalise the section of the trace containing D.W.W. arrivals independently of the large amplitude bottom reflection. This proceedure allowed the D.W.W. to be timed to better than 1mm or 13 ms for these shots.

Along the refraction part of the profile, the D.W.W. could be timed to better than 0.5 mm (7ms) for all shots closer than 25 km. In the range 25-55 km, the D.W.W. became very emergent and I found it easier to time the bottom bounce instead. By assuming a value for the water depth at the middle of the shot, it was then possible to calculate the shot-receiver distance. Once again the lack of adequate depth sounding was the major source of error, with the poor assumption of the depth being the limiting factor in the accuracy. It was possible on some shots to time both the D.W.W. and the bottom bounce. In these cases, the two results agreed to within 50 m for all cases tested. Beyond 55 km, the

D.W.W. and the bottom reflection arrived so close together as to be indistinguishable. The combined phases were somewhat emergent from the background noise of late refraction arrivals and reverberations, causing the first break in these cases to be determined to better than 4mm or 50 ms.

The total error calculated for the shot-receiver distance incorporates not only the timing error of the D.W.W. and bottom reflections, but also the error in the origin time. The total estimated error in the shot-receiver distances are therefore :

TABLE 2.1

Reflection Data

Distance Range km	Shot Depth m	Timing Error ms	Distance Error m
0-2	7	<22	<30
2-4	7	<30	<45
0-4	45	<22	<30

Refraction Data

Distance Range km	Timing Error ms	Distance Error m
5-25	<22	<30
25-55	<70	<100
55-95	<120	<200

Thus in all cases the distances could be determined to better than 1.5% and in most cases to better than 1%.

2.4 Record Sections

Record sections of all reflection and refraction profiles were compiled using the program RSEC written by the author and now available for general use. As one might expect, it was not sufficient to simply compile the raw demultiplexed data since any amplitude information would be lost if no appropriate corrections were applied. To obtain meaningful information from the amplitudes it was neccessary to compensate for the effect of spherical spreading, varying charge size and varying amplifier gain.

Amplifier Gain :

The ambient noise level at each hydrophone varied greatly due to the positioning of the main cable and manouvering of the ship. In order to maintain a similar background noise level on all traces and to prevent the transient noise impulses (especially at high gain) from overloading the amplifiers, different gains were used on different amplifiers. The gain (G) is defined by :

$G=20\,\mathrm{Log}(V_{out})$

V_{out}=output voltage for a 1 volt input

To remove this effect a correction of $10^{\frac{-G}{20}}$ was applied to all traces, in effect normalising all amplitudes to a chosen constant gain.

Charge Size :

For a charge weight of W pounds, O'Brien (1960) and Mueller (1962) have shown that seismic amplitudes recorded at sea vary approximately as $W^{2/3}$. In order to remove the effect on amplitudes of using various charge sizes along the profiles, corrections of $W^{-2/3}$ were applied to all traces for a single shot.

For the reflection profiles and out to a distance of 67 km (shot 54) on the refraction profiles, commercial explosives were used as energy sources. Beyond 67 km, however, the energy source for each shot consisted of three anti-submarine projectiles having an equivalent yield of 282 kg. There probably exists a difference in energy yield between the bombs and the commercial explosives due to the different explosive types and the steel packaging of the bombs. However, no correction for this difference has been made, but it should be noted.

Spherical Spreading :

Cerveny and Ravindra (1971) have shown that head wave amplitudes at large distances decrease as $1/r^2$; near the critical distance, however, the drop in amplitude is closer to $1/r^3$ or $1/r^4$. Even so, it was decided to apply a uniform amplitude correction of r^2 to the refraction seismograms to correct for spherical spreading. This is not entirely appropriate as Braille and Smith (1975) have shown that wide angle reflection amplitudes decrease as $1/r$. Thus the r^2

factor will enlarge these amplitudes out of proportion to the refraction amplitudes. However these same corrections are applied to the synthetic seismograms so the compensation is consistent.

To compensate for the effect of spherical spreading on the sub-critical reflection data a factor of r^1 was applied to the data. This is also not entirely appropriate, Braille and Smith (1975) having shown that reflection amplitudes in a layered medium drop off between r^{-1} and $r^{-1.5}$. It was decided however that a correction of r^1 was satisfactory since amplitudes were not being used in other than a qualitative manner.

Hydrophone Sensitivities :

Two of the hydrophones were new and unused whereas the others were purchased a few years before and had been used to varying extents on previous trips. Both age and extent of use tend to affect the sensing element; as a result, the hydrophones were of differing sensitivities. Consequently, after all the other corrections had been applied the traces from each channel for a particular shot differed significantly in amplitude. As a correction for this effect, the amplitude of each channel was multiplied by an appropriate correction factor to approximate a constant amplitude for a given phase.

It is desirable in the compilation of any marine seismic record section to remove the effect on travel times of the varying bottom topography. I have mentioned several times

previously that we did not have adequate depth sounding on the cruise. Without wishing to belabour the point, the lack of such information plus the relatively smooth topography along the profile (see Fig 1.2) made the application of static corrections unnecessary.

Although the first profile was started with six functioning hydrophones, as one might expect, we did not finish with the same number. Channel two became inoperative midway along profile 75-1R (recorded first) and remained so for the duration of profile 75-1. Channel six also threatened to cease functioning at the start of 75-1; however, it did operate off and on for the duration of the profile thus giving usable information at irregular intervals. All data from inoperative hydrophones were ignored during the compilation of the record sections.

Prior to final compilation into record sections, the data were bandpass filtered using a zero phase, four pole Butterworth filter. An excellent development of the theory for Butterworth filters is given in Kanasewich (1976). The analog amplifiers provided filtering between 0.8 and 100 hz, but this was judged to be insufficient as a considerable amount of high frequency noise remained. In order to remove this noise and improve the general apearance of the sections all seismic traces were filtered between 5.0 and 30 hz.

Filtering limits of 2.0 to 15 hz were applied at one stage to various sections of profile 75-1. This was done in an effort to identify later arrivals embedded in the

reverberations of earlier arrivals. This proceedure proved quite successful as shown by Fig 4.8 where coherent later arrivals were identified.

The program RSEC is capable of compiling and plotting any part of a complete record section with any desired time and distance scale, and any desired amplitude. This proved to be a most useful tool in analysing the seismic data. The ability to look at any individual portion of a complete section at any desired amplitude saved considerable time throughout the analysis of both reflection and refraction profiles.

3 SUB-CRITICAL REFLECTION DATA

3.1 Methods of Analysis

The record sections for reflection profiles 75-1R and 75-1 are shown in Figs 3.1 and 3.2, respectively. These profiles contain all the data available from the operative hydrophones. The first arrival seen on the profiles is the direct water wave. Both the first and second bottom bounces can be identified, the first starting at about 2.7 s and the second at about 5.3 s. All of the reflections timed for analysis are shown on the profiles, although the ones shown with a "?" on Fig 3.1 were too poorly defined to allow proper analysis. These record sections were very useful in gaining a broad overview of the reflecting sequences. However they were not particularly useful in identifying and timing individual arrivals due to trace overlap, hydrophone signature variations and the generally cluttered appearance. Far more detail was needed to time the arrivals than could be obtained off these complete sections.

Fig 3.3 shows the type of section used to identify and time arrivals. By using these expanded sections it was possible to examine sets of arrivals for one channel at a time. As previously mentioned, the hydrophones were of different ages, resulting in different frequency responses for each one. This differing frequency response was responsible for each channel having a different arrival signature. With

Fig 3.1

Record section of reflection profile 75-1R using shots at 45m depth. Amplitude corrections have been applied to the data as per section 2.4 and the data are filtered 5.0-30 hz. The part of the section within the rectangle is shown on the right side with a five-fold increase in amplitude. The DWW arrival lies along the straight line. Curved lines show the six reflection phase correlations which were timed. W is the bottom reflection. The dashed line shows the transition from a deep reflector to the first refraction arrival. The "?" indicates poorly defined reflections.

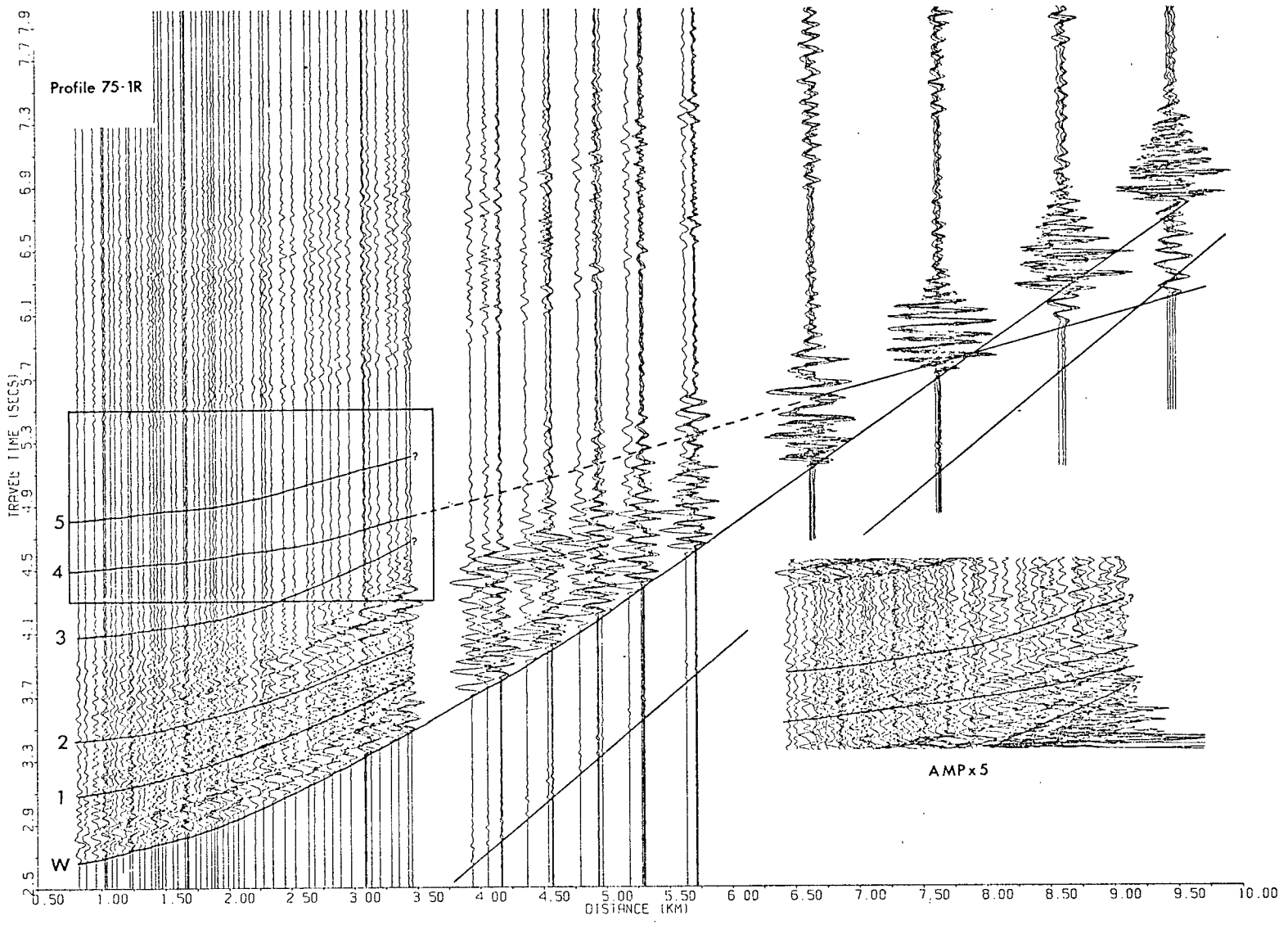
Profile 75-1R
TRAVEL TIME (SECS)
2.5
2.9
3.3
3.7
4.1
4.5
4.9
5.3
5.7
6.1
6.5
6.9
7.3
7.7
7.9
W
1
2
3
4
5
?
?
AMP x 5
0.50
1.00
1.50
2.00
2.50
3.00
3.50
4.00
4.50
5.00
5.50
6.00
6.50
7.00
7.50
8.00
8.50
9.00
9.50
10.00
DISTANCE (KM)

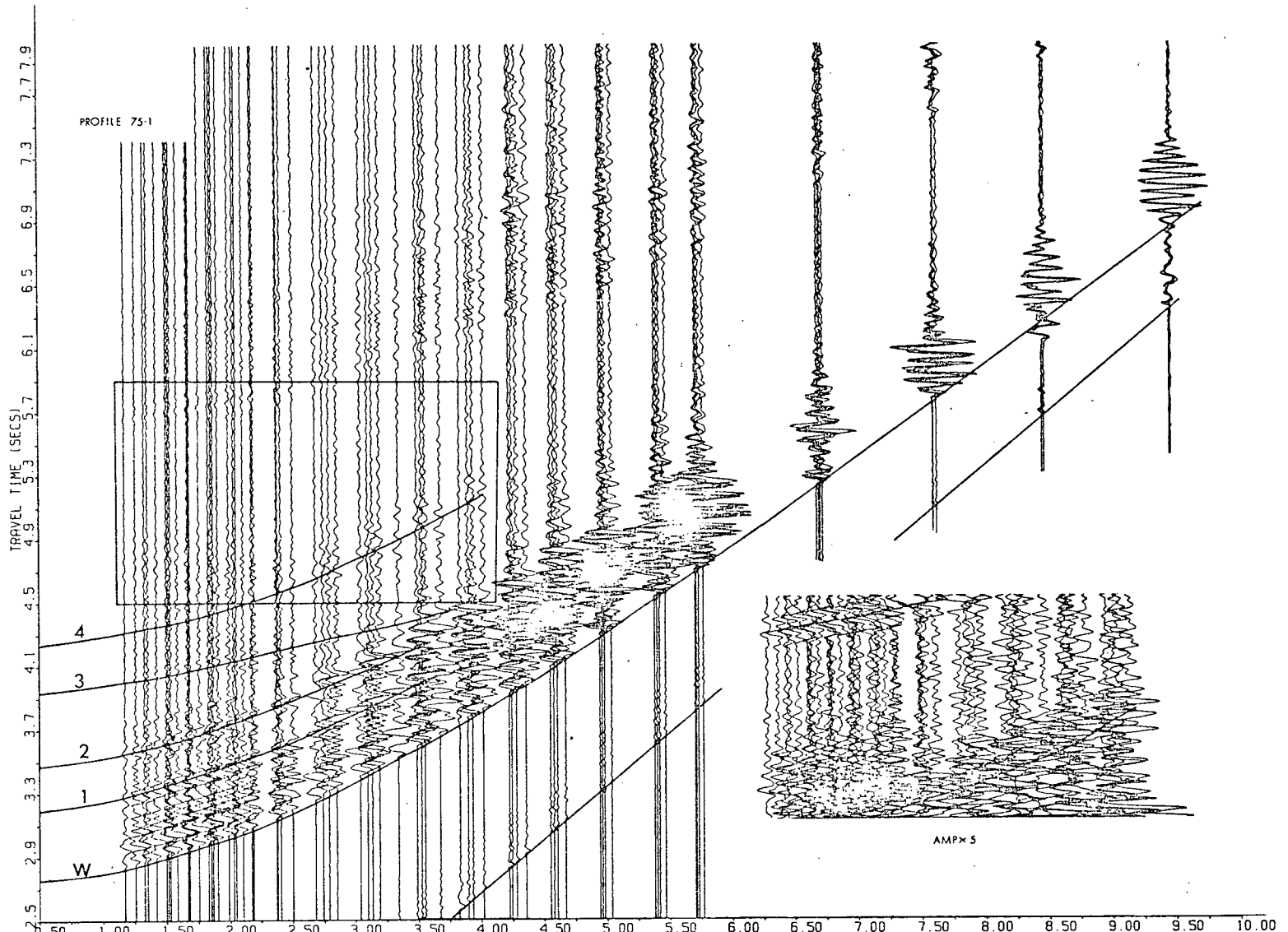

Fig 3.2. Same as Fig 3.1, for profile 75-1.

all channels plotted out together as in Figs 3.1 and 3.2, I found it extremely difficult to phase correlate arrivals due to the differing signature complicating any continuity in the phases. However with the individual channel sections, phase correlations could be accomplished quite easily. This differing arrival signature is shown clearly on Fig 3.3.

Even using the smaller sections I encountered a number of problems, the major one being the approximately 300 ms length of the arrival signatures. This was caused by a prominent bubble pulse with period of approximately 100 ms. The D.W.W. arrival seen on Fig 2.1 (B) and on Figs 3.1 and 3.2 show clearly this bubble pulse problem. Both the first and second bubble pulses had sufficient amplitude to complicate the records, the first bubble having a relative amplitude of 0.9 and the second a relative amplitude of 0.4, when compared to the original pulse. This effect tended to obliterate everything within 100 ms of the onset of an arrival.

Various deconvolution methods have been attempted on similar data by Knize (1976). His conclusion was that time adaptive deconvolution would be required to reduce this bubble pulse effect and enhance the data. This falls beyond the scope of this project with the result that no deconvolution has been attempted.

One other minor problem with the sections is the marked decrease in amplitude of the signal along the trace. This makes later arrivals difficult to see if the complete trace is plotted. This was solved quite simply by splitting the section

Fig 3.3

Two typical record sections used to time individual reflection arrivals. Both sections are filtered 5.0-30 hz. The correlated phases are the water bottom and first and second sub-bottom reflectors.

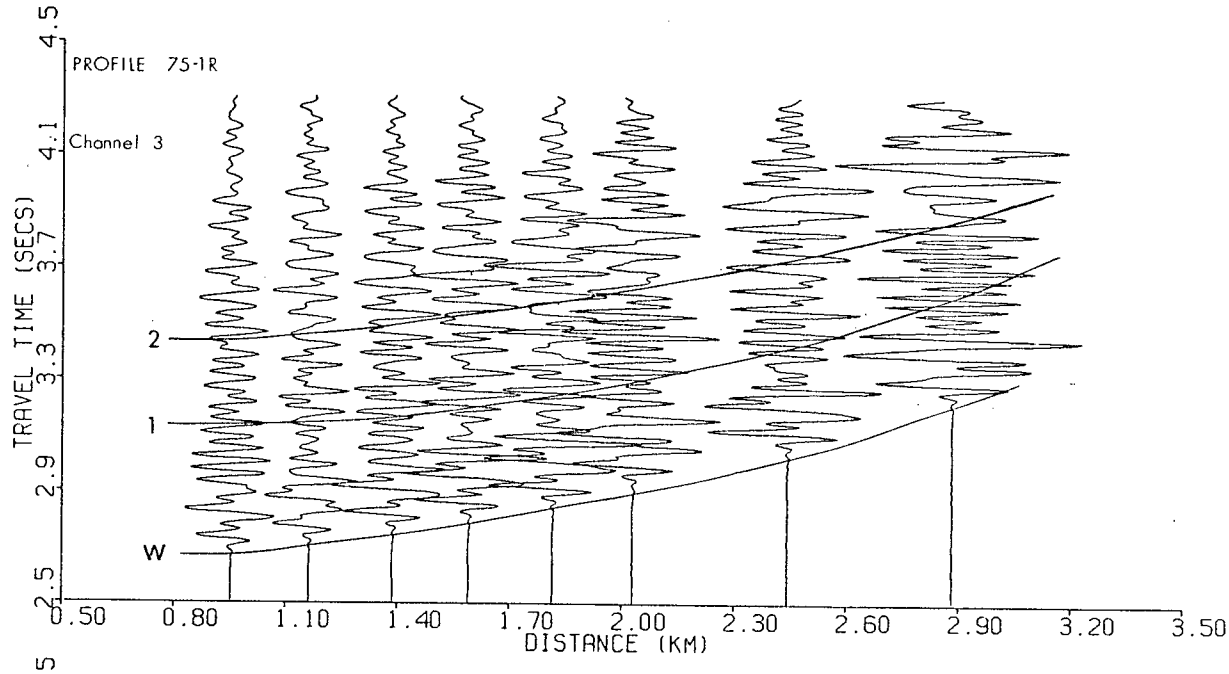
PROFILE 75-1R
Channel 3
TRAVEL TIME (SECS)
4.5
4.1
3.7
3.3
2.9
2.5
2
1
W
0.50
0.80
1.10
1.40
1.70
2.00
2.30
2.60
2.90
3.20
3.50
DISTANCE (KM)

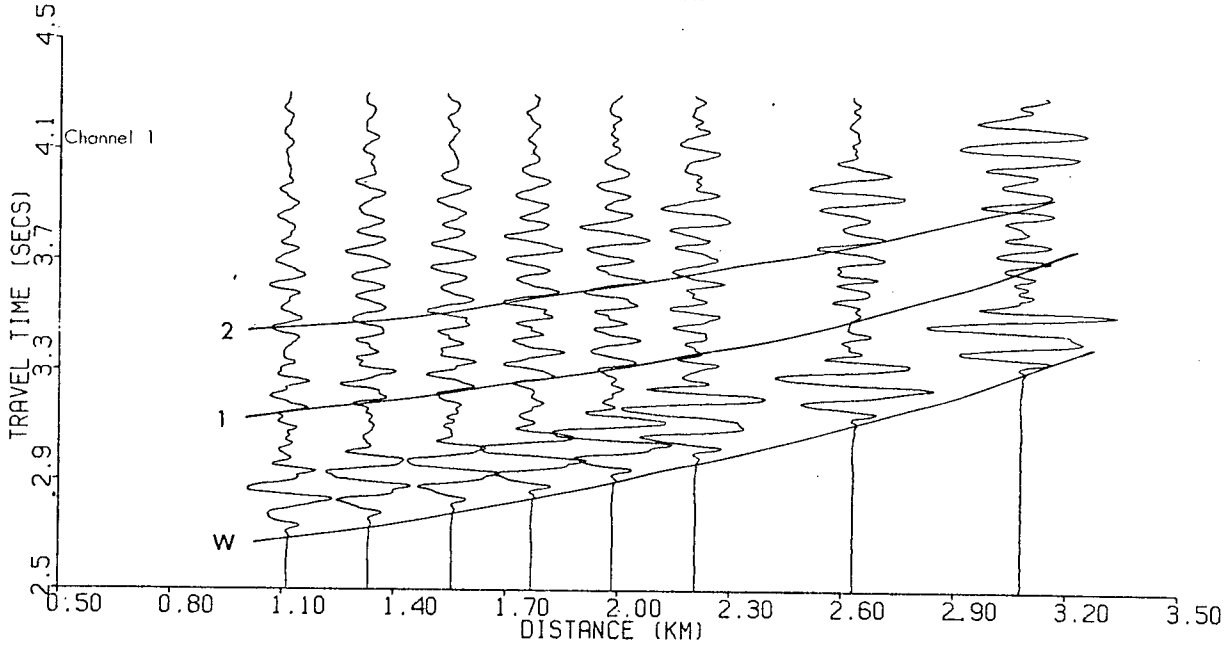
Channel 1
TRAVEL TIME (SECS)
4.5
4.1
3.7
3.3
2.9
2.5
2
1
W
0.50
0.80
1.10
1.40
1.70
2.00
2.30
2.60
2.90
3.20
3.50
DISTANCE (KM)

into various time segments and by plotting out each time section individually with an appropriate amplitude.

Any reflection interpretation from which velocity information will be calculated is only as good as the timing of the various arrivals. As stated previously, I was able to phase correlate arrivals from shot to shot using record sections showing only one channel at a time. Phase correlation of arrivals between different channels for the same shot however was not possible. Thus the phases picked for the various channels were sometimes offset from one another by as much as 50 ms. Corrections for these offsets were made by overlapping the various sections on a light table and measuring the time difference between the phases picked on each channel relative to a standard channel. By this method I was able to eliminate the problem of picking different phases for each channel.

While it was possible to trace arrivals out to approximately 3.0 to 3.5 km it was impossible to pick first breaks. Most arrivals were extremely emergent from the reverberations and bubble pulses of earlier arrivals. Thus their first breaks were essentially hidden. As a result, all picks for any one arrival could be offset by up to 50 ms from the first break. No attempt was made to correct for this, however, as it was difficult to identify just what the offset time should be. This offset, while not affecting the layer velocities obtained in the analysis, placed limits of 50 to 100 m on the layer depths.

Finally, although I had considerable success phase correlating arrivals, at distances beyond 2.5 km the arrivals from the different horizons started to overlap somewhat. This caused considerable confusion in trying to follow phases with the result that the possibility of "jumping" a phase cannot be overlooked.

Once the arrivals had been timed I was faced with the problem of how to analyse the data obtained. The basic problem is that the travel time of the arrivals is related to the average velocity from a plane containing the shot and receiver to a reflecting horizon. In our case this average velocity is dominated by the thick water layer (2000 m) causing the average velocity to change very little from layer to layer. In order to analyse the results of the travel time picks, it became essential to remove the effect on the various arrivals of this thick water layer. Three methods have been used to accomplish this.

1) Ray Parameter Method :

The ray parameter (p) of a seismic ray can be thought of as the angular velocity of turning about the centre of the earth of the ray in question. If we assume the earth is laterally homogeneous (an assumption that is made in most refraction and reflection analyses), then the ray parameter (R.P.) remains constant along the ray path. This makes it extremely suitable as a tool for analysing both reflection and refraction work.

Consider the following :

A)

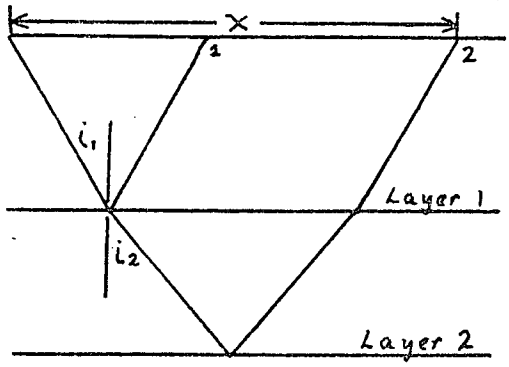

B)

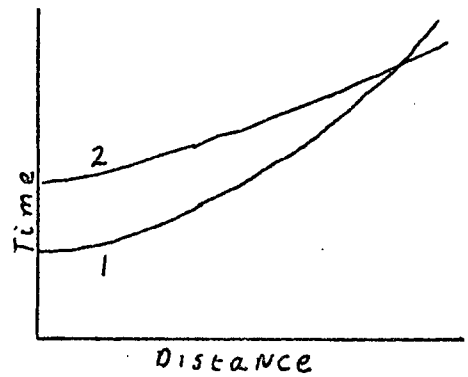

$$p=\sin(i)/v \qquad 3.1\text{-}1$$

$$p=dT/dX \qquad 3.1\text{-}2$$

According to Snell's law $\sin(i_1)/v_1=\sin(i_2)/v_2$. Hence 3.1-1 is simply a restatement of Snell's law. 3.1-2 is derived by Bullen (1963, p 110) and is the fundamental equation of the ray parameter method

The two layered medium of diagram (A) results in the two T vs X curves of diagram (B). The curve defining arrival 2 is comprised of contributions from the passage of the rays through both layers one and two. The objective is to remove the effect on the second T vs X curve, generated by the reflection of the ray off the bottom of layer 2, of the ray passing through layer one. This can be accomplished quite simply by using eqn 3.1-2.

Equation 3.1-2 states that the p value corresponding to an arrival at a distance X equals the slope of the travel time

curve (T vs X) at that point. It is possible then to obtain a p vs X curve for both arrivals one and two by fitting the curves (T vs X) with a third order polynomial and then taking the derivative of the fitted curves. Any particular ray with R.P. value p will arrive at the surface after reflecting off both the first and second layers. By subtracting the travel times and distances obtained from the corresponding p values on the two T vs X curves we can remove the effect on the ray of its passage through layer one. We have then reduced the arrival to a simple one layered case which may be analysed by the standard formula given below

$$T^2=(X^2+4H^2)/V^2 \qquad 3.1\text{-}3$$

Where H=depth of the layer

V=velocity of the layer

Keen (1976) has devised an algorithm to perform the above analysis. I have modified this algorithm to fit my own data and have used it as the primary method of reducing the reflection data.

T^2-X^2 Method :

Having had no previous experience with the ray parameter method, I thought it better to compare the results obtained using it with results obtained using the more familiar T^2-X^2 method.

Dix (1955) has defined the average root-mean square (r.m.s.) velocity from the surface down to the bottom of the

nth layer as

$$\bar{V}_N^2 = \frac{\sum_i^N \bar{V}_i^2 T_{o,i}}{\sum T_{o,i}} \qquad 3.1\text{-}4$$

Where $\bar{V}_N$ is the average r.m.s. velocity

$\bar{V}i$ is the interval velocity of the ith layer

$T_{o,i}$ is the two-way vertical incidence travel time in the ith layer.

When the travel times and distances of a set of arrivals from one reflecting horizon are plotted on a T vs X curve they are hyperbolic. If, however, they are plotted on a T^2-X^2 curve, they define straight lines, the intercept being the two way vertical incidence travel time and the inverse slope being the average r.m.s. velocity of the arrival. This velocity corresponds to $\bar{V}_N$ of equation 3.1-4.

Let us now define the average r.m.s. velocity from the surface to the top of the kth layer and its corresponding two way vertical incidence travel time as $\bar{V}_{K-1}$ and T_{K-1}. Let us further define $\bar{V}_K$ and T_K as being the corresponding values to the bottom of the kth layer. Then the interval velocity of the kth layer is given by Dix (1955) as :

$$V_K^2 = \frac{\bar{V}_K^2 T_K - \bar{V}_{K-1}^2 T_{K-1}}{T_K - T_{K-1}} \qquad 3.1\text{-}5$$

Equation 3.1-5 has been used to generate a velocity depth model to compare with the results obtained using the ray parameter method.

3) Stripped T^2-X^2 Method :

A third method of analysis, hereby referred to as the stripped T^2-X^2 method, was attempted. This method, unlike the previous two, depends on the previous calculation of the upper layer velocities and depths.

I used the ray parameter method to the extent of obtaining the p vs X curve for the arrival branch in question. The upper layers however were stripped off by means of equation 3.1-1 and simple geometry. Once the upper layers had been stripped off the remaining data were analysed by use of equation 3.1-3

The major problem associated with this method is that it requires an accurate knowledge of all the layer velocities and depths above the layer in question. These velocities and depths are also calculated by this method, resulting in a step by step progression in the analysis. Unfortunately this also means that any errors encountered during the calculation of the velocity and thickness for a layer will affect the subsequent values for all the lower layers, with the errors accumulating from layer to layer. We would expect therefore that this method would become less and less accurate with each additional layer. This method was attempted more for my own edification than for the results obtained. It was not expected that it would yield usable solutions from the data.

3.2 Analysis of Results

Profile 75-1R

Fig 3.1 shows the complete record section of reflection data for profile 75-1R using shots at 45 m depth. The profile using shots at 7 m depth was also compiled; however, it added little to the analysis as the lower energy yield of the 7 m shots did not allow the depth of penetration of the 45 m shots. For this reason the profiles using shots at 7 m were not analysed. A total of five sub-bottom reflectors are identified on Fig 3.1; unfortunately only 3 could be timed sufficiently well to be analyzed.

The first two reflectors are clearly identified and little trouble was encountered in timing them. There is a prominent arrival approximately 300 ms after reflector two. This, however, was identified as either a reverberation or a bubble pulse effect as it had the same moveout as reflector two. Both reflectors one and two are seen clearly upon examination of the water bottom multiples beginning at a time of approximately 5.3 s. This gives further evidence for their being interpreted as separate arrivals.

The timing of of arrival three was too poor to enable any sort of proper analysis. As a result it is identified on Fig 3.1 with a "?". This arrival could also be seen on profile 75-1; however, once again it also was not usable due to poor timing.

Reflector four is timed very well and can be identified as the reflection from the sediment/basement interface, since it can be traced out to the first refraction arrival (apparent velocity of 4.28 km/s). This transformation from the reflection to the refraction arrival is shown on Fig 3.1 with a dashed line.

Reflector five is the last reflection that can be identified as a separate arrival. Unfortunately it is too weak to time. It is my opinion that it is an arrival from a deeper crustal layer, but due to the lack of adequate timing this idea can not be supported.

The arrival times and distances for the water bottom reflection and reflectors one, two and four in both T vs X and T^2 vs x^2 modes are plotted on Fig 3.4 (A) and (B), respectively. I have also plotted the arrival times of reflector three on these plots to illustrate how inadequately this arrival is defined. Table 3.1 compares the results of the analysis of the usable arrivals using the three methods discussed in the last section.

The ray parameter and T^2-X^2 methods yield essentially identical results and comparable errors. The stripped T^2-X^2 method results differed from the previous two to a greater extent, especially in the last layer. This is consistent with what would be expected considering that the errors in this method are cumulative. The first two methods are similar in that neither method requires any previous knowledge of the velocities and depths of the layers above the one in question.

Fig 3.4

A. T vs X plot for 5 reflections from profile 75-1R shown on Fig 3.1. The lines are third-order polynomial fits used in the ray parameter method of determining velocities and depths.

B. T^2 vs X^2 plots for the same data. The lines are least squares fits used in the T^2-X^2 method of analysis.

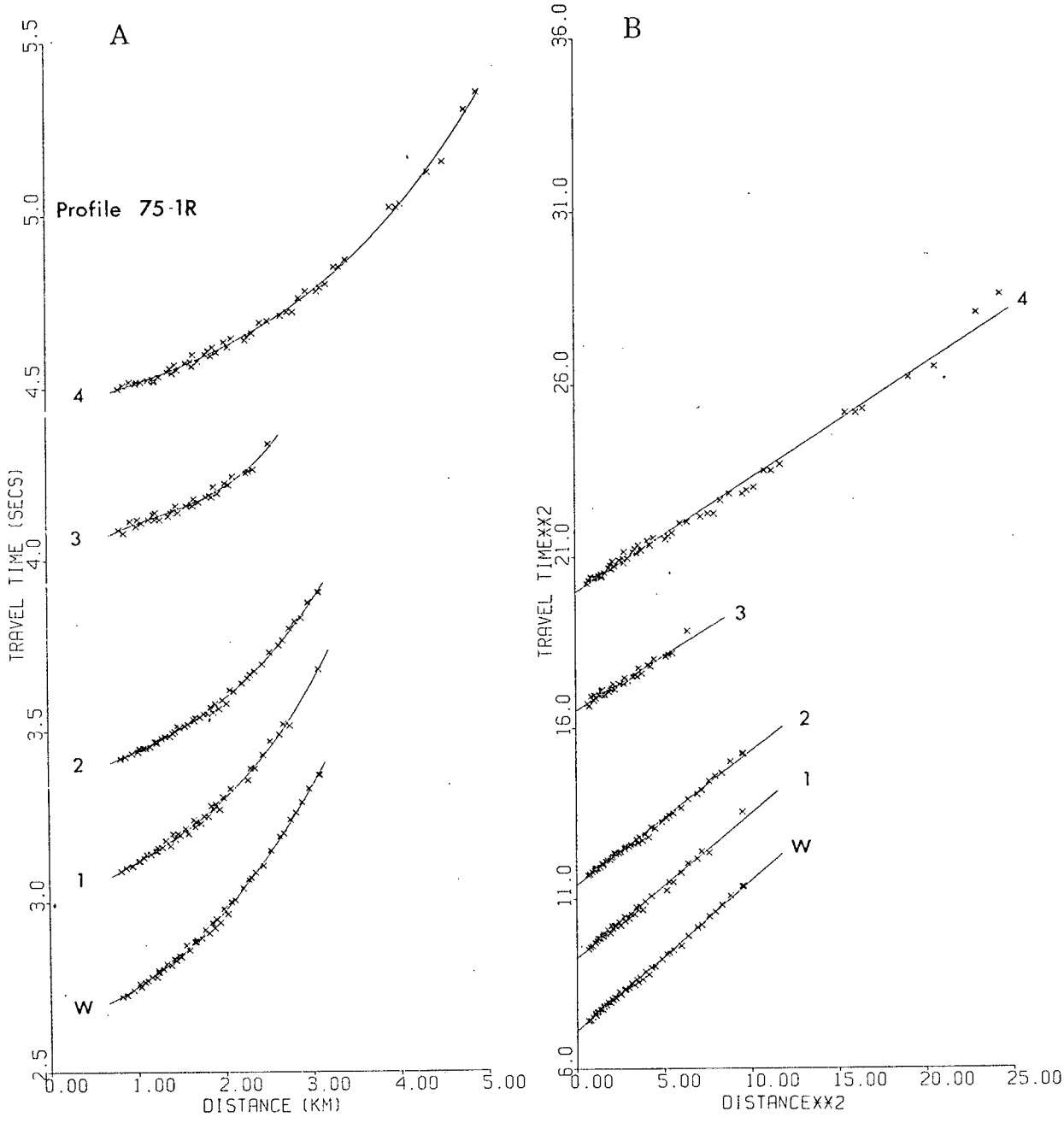
A
Profile 75-1R
TRAVEL TIME (SECS)
DISTANCE (KM)
4
3
2
1
W
B
TRAVEL TIMEXX2
DISTANCEXX2

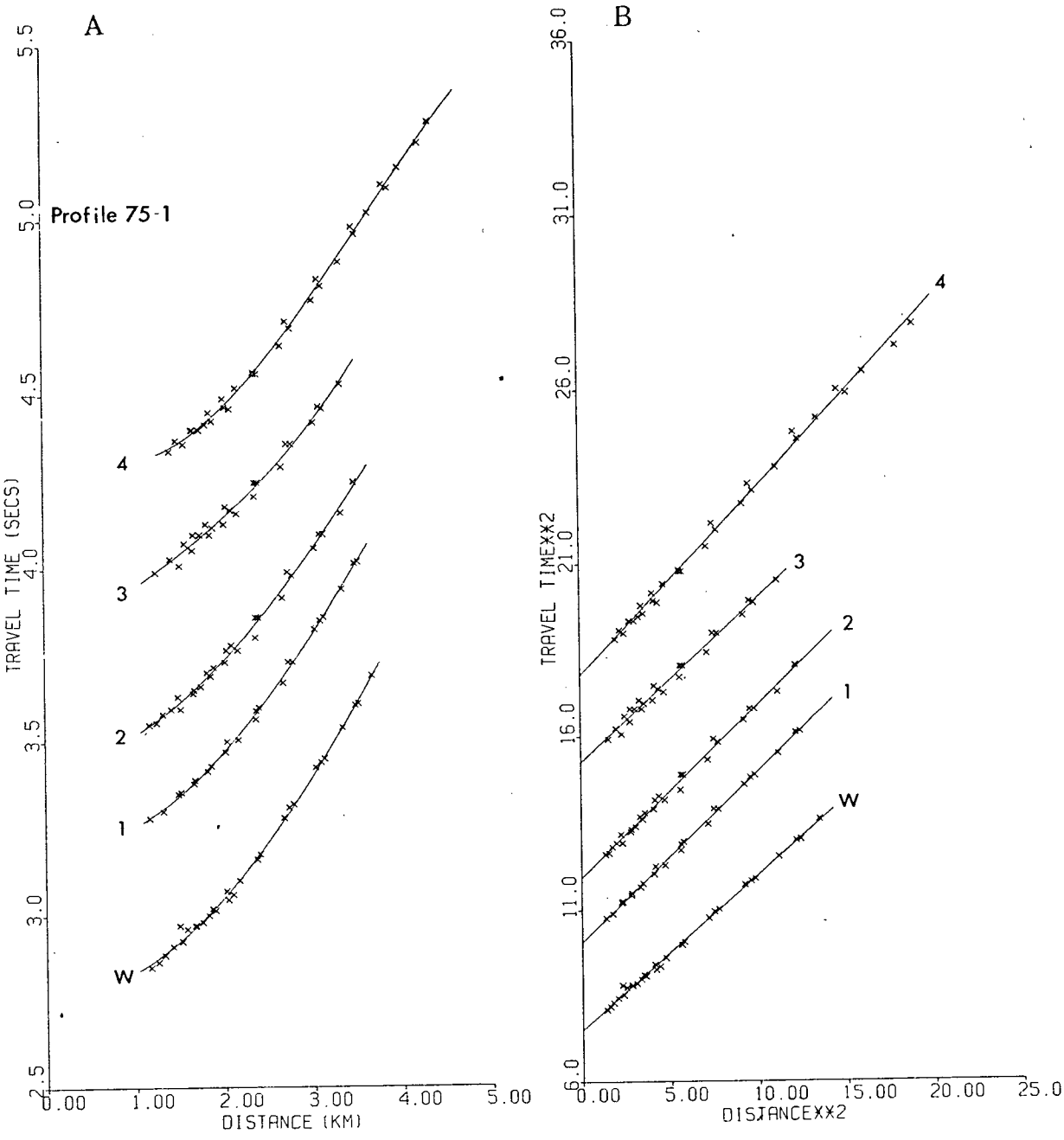

Fig 3.5, same as 3.4, for profile 75-1

TABLE 3.1

Profile 75-1R

	Ray Parameter	T^2-X^2	Stripped T^2-X^2
Water (surface to W)			
Velocity		1.50 ± 0.01	
Thickness		1.95 ± 0.01	
Sediments			
Layer 1 (W to 1)			
Velocity	1.79 ± 0.08	1.76 ± 0.05	1.68 ± 0.11
Thickness	0.33 ± 0.01	0.34 ± 0.01	0.30 ± 0.02
Layer 2 (1 to 2)			
Velocity	2.02 ± 0.06	2.01 ± 0.05	2.08 ± 0.10
Thickness	0.32 ± 0.01	0.33 ± 0.01	0.35 ± 0.02
Layer 3 (2 to 4)			
Velocity	2.14 ± 0.03	2.12 ± 0.05	2.16 ± 1.26
Thickness	1.17 ± 0.02	1.15 ± 0.01	0.74 ± 0.44

All velocities are in km/s and all thicknesses are in km.

As a result, inaccuracies in calculating the velocity and depth of a layer will not affect the results calculated for deeper layers. This is in direct contrast with the stripped T^2-X^2 method that propagates errors from one layer to the next. From this we would expect the results between all three methods to agree fairly well for the first layer or two. As the number of layers increases, however, the last method will become progressivly less accurate due to the accumulation of errors.

The velocity vs depth results from the analysis of sediment reflections for profile 75-1R are given in table 3.2.

TABLE 3.2

Layer	Velocity (km/s)	Thickness (km)	Depth to Top of Layer (km)
Water	1.50 ± 0.02	2.00 ± 0.01	0.0
Layer 1	1.79 ± 0.08	0.33 ± 0.01	2.00
Layer 2	2.02 ± 0.06	0.32 ± 0.01	2.33
Layer 3	2.14 ± 0.03	1.17 ± 0.02	2.65
Oceanic basement			3.82

By placing the shots at 45m depth for this profile we have managed to penetrate to the base of the sediments without obliterating the immediate sub-bottom arrivals. The profiles

using shots at 7 m depth provided essentially the same information, but for only approximately 1.5 s of penetration (2-way). For this reason I do not recommend that such profiles be recorded in future work as they add little to the analysis.

It may be possible that we do have reflections from deeper basement layers. Unfortunately, if they are present they are of so low an amplitude as to be indistinquishable from background noise and the water bottom multiples. This, for example, could be the case with reflector five identified with a "?" as the last reflector on Fig 3.1. It has been suggested that velocity (w-k) filtering (Trietel et al 1967) might enhance these arrivals. This method of filtering was not initially designed for our type of data as it has the requirements that the spacing between traces be uniform, and that the arrivals have a uniform moveout per channel. That is, when plotted on a T vs X graph the arrivals should yield a straight line. Since the hydrophone array was allowed to be more or less free moving to lessen the ambient noise, the first condition is not met. Also, for this type of reflection work the T vs X plots of the arrivals are hyperbolic and not linear and thus the data does not fit the second criteria. Even so, I have attempted to expand the w-k method to fit this type of data. This was done as a project for the course, Geophysics 514, "Time Series Analysis", given by Dr T. J. Ulrych and was intended only as a feasability study. The results, while being far from conclusive, do indicate that it may be possible to expand w-k filtering to this type of data,

even considering the problems just discussed. I shall leave this as a legacy for a subsequent adventurous student.

The velocity depth model just given should not be considered as absolute. Due to the non-reversal of the data the velocities are only "apparent" velocities and not the true interval velocities. The presence of dipping layers can greatly affect the velocity measured for a layer as all the methods of analysis assume that the layers are homogeneous and flat lying. This will be expanded upon during the discussion of the 75-1 reflection profiles where dipping layers cause the results to be meaningless.

As mentioned in Chapter 1, C.S.P. data were acquired during this cruise. C.S.P. line 75-1 (Fig 1.3) at its northwest end closely parallels the reflection line while C.S.P. line 75-3 (Fig 1.4) runs perpendicular to it being approximately 30 km southeast. Both profiles clearly show the presence of definite layering in the sediments, with considerable evidence for folding of the layers. However, this folding does not appear to have disrupted the continuity of the layers. An attempt was made to correlate the arrivals timed on the reflection profiles with the C.S.P. profiles. The C.S.P. data however only penetrated to about 4 s two way travel time. Even so, I was able to make a tentative correlation between prominent arrivals on the C.S.P. and the first two sub-bottom reflectors, although precise layer correlations could not be made. Profile 75-1R is somewhat to the northwest of the end of C.S.P. line 75-1. For this reason,

it is not possible to identify the precise magnitude of the dips present in the region of 75-1R. From the C.S.P. data that we do have though, I think it is safe to assume that the dips in the region will be of the order of one to two degrees. Just what changes these dips will make to the layer thicknesses and velocities is difficult to determine because of the complex layering present. Any changes produced though should not be too great, being of the order of 2 to 4%. For this reason a mild caution is placed on the reflection results for profile 75-1R.

The main purpose behind the reflection surveys has been to obtain a reasonable picture of the sediments for use in the analysis of the refraction data section, and to obtain a more accurate total depth for the sediments than has previously been reported by such authors as Tiffin (1972) and Couch (1969). The total sediment thickness obtained from the analysis of profile 75-1R is approximately 1.8 km. Even considering that the layers are dipping at an unknown angle and making generous allowance for this possibility, the sediment thickness is not likely to be inaccurate by more than 200 m.

Profile 75-1

The complete set of reflection data for profile 75-1 using shots at 45 m depth is shown in Fig 3.2 If we compare it directly to Fig 3.1, the similar section for 75-1R, we can see immediately that the arrivals timed on 75-1 are somewhat

questionable. Some of the arrivals shown on Fig 3.2 do not appear as coherent as the corresponding arrivals on Fig 3.1. I was able to time what I interpreted as the same reflectors as on 75-1R, except I was not able to time the last reflector, or even see it on this profile. These arrivals were identified as being from the same reflectors on the basis that they had similar travel time spacing and relative amplitudes as on 75-1R. The major difference between the two profiles can be seen by comparing the T vs X and T^2-X^2 plots for both profiles (Figs 3.3 and 3.4). The results for profile 75-1 are unusual in that they indicate that the average velocity to a layer decreases with depth, with all the average velocities being lower than that of water. This can be seen clearly on Fig 3.5 where the slopes of the T^2-X^2 lines increase from one layer to the next. The slopes and intercepts of the lines are given Table 3.3.

TABLE 3.3

	Water	Branch 1	Branch 2	Branch 3	Branch 4
Velocity km	1.49	1.42	1.42	1.45	1.35
Intercept s^2	7.54	10.06	11.92	15.25	17.78

The reason for these non sensical results has already been introduced during the discussion of profile 75-1R, that being the presence of dipping layers. All of the three analysis methods discussed previously assume flat lying layers, for this reason they could not be used to analyse this profile. The only way of obtaining any useful information from this profile is to assume that the velocities and depths given by the 75-1R profile also applied here. Then it is possible to determine the dips that would give rise to the results obtained. This was done to obtain the approximate dip for the first sub-bottom reflector. A model based on the diagram below was used and the "apparent" average velocity to the reflector was calculated using various values for θ,

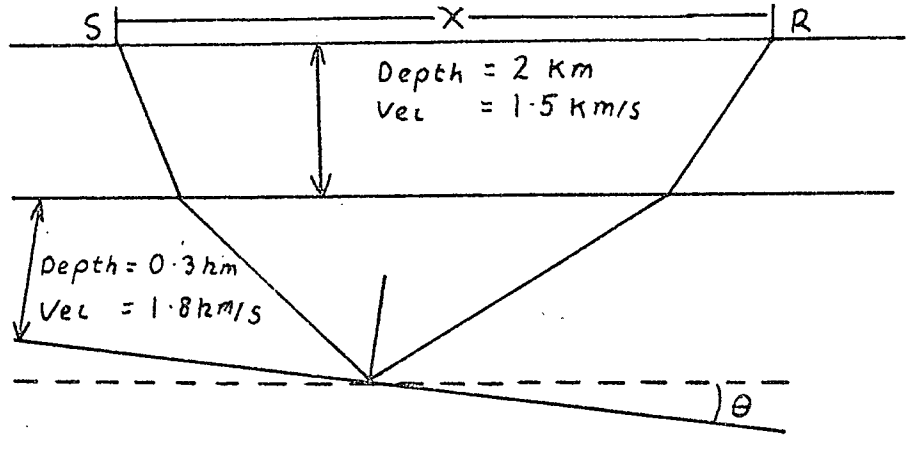

The calculation showed that values of θ ranging from five to ten degrees would yield a velocity for the arrival similar to the 1.42 km/s velocity obtained from the T^2-X^2 plot for the average velocity to the first reflector.

It now remains to be seen if the sediments in the region of profile 75-1 have dips of this order. Our own C.S.P. line 75-1 (Fig 1.3) does not give any clear details of the

sediments at the southeast end of the profile. Murray and Tiffin (1976), however, have published a C.S.P. profile (Fig 1.5) which almost directly overlaps our region of interest. As can be seen, the sediments in this region are highly folded. The distinct layering present at the northwest end of the profile is not as evident, and the sediments are folded more drastically, the amplitude of folding increasing with depth. From the C.S.P. data, calculation of the dips in this region, range from approximately +10 to -10 degrees, and hence agree with the values of the dips required to make the first layer apparent velocity agree with that determined from the T^2-X^2 analysis.

4 REFRACTION DATA ANALYSIS

4.1 First Arrival Interpretation.

Until recently the only method used to analyse marine refraction data was the so called "First Arrival Method". This type of analysis, while being very easy and quick to perform, does not take into account the secondary arrivals and dynamic amplitude aspects of the data. The advent of sophisticated but relatively inexpensive methods of calculating synthetic seismograms has enabled the expansion of marine refraction interpretations to include amplitude information as well as the complete travel time data set. The first arrival method remains as a valuable tool, however. Its major use now is in generating a preliminary velocity depth model for use as an initial interpretive guide and as a starting model for the generation of synthetic seismograms. For this reason, a first arrival interpretation of the data was the first step in the interpretive procedure used in this study.

The seismograms used in timing the first arrivals are the same ones used to time the direct water wave phases, which in turn give the shot-receiver distances. The timing method for first arrivals was identical to that used for the D.W.W. (see section 2.3 and Fig 2.1).

To a distance of 55 km on profile 75-1R and 65 km on 75-1, the signal/noise ratio was high enough to enable the timing of first breaks to better than 1 mm or 15 ms. The

signal/noise ratio lessened at this point and consequently over the range 55-75 km on 75-1R and for the rest of the profile on 75-1, an accuracy of better than 2 mm or 30 ms has been attributed to the picks. Beyond 75 km on 75-1R the signal amplitudes were too low to enable arrrivals to be timed to any reasonable degree of accuracy.

Fig 4.1 is the reduced traveltime plot for first arrival data for both profiles 75-1 and 75-1R, the reducing velocity being 6 km/s. An expanded plot of the first two phases (i.e. 8-28 km) is shown on Fig 4.2. This plot shows how well the first two sets of arrivals are defined.

Let us now examine Fig 4.1 in greater detail. The first thing to note is the great degree of similarity between the two profiles, the main difference being an offset of approximately 200 ms between them. The layer velocities given by the inverse of the slopes of the least-squares lines are also in excellent agreement, indicating that there is little dip on the refracting horizons.

For both profiles, the first set of arrivals start at approximately 9 km and persist for about the next 5 km, with a least-squares velocity of approximately 4.28 km/s. At about 14 km, the next branch (5.26 km/s) becomes the first arrival and persists as such for the next 15 km . Once again this travel time branch is extremely well defined, as shown by Fig 4.2. Over the distance range 29-44 km on both profiles, the 6.28 km/s travel time branch becomes the first arrival. This branch is not as well defined as the previous two, being defined by

Fig 4.1

Reduced travel time data and least squares fitted lines for both refraction profiles. The reducing velocity is 6 km/s. Inverse slopes are the velocities in kilometers per second; intercepts are in seconds. Triangles show data for the profile 75-1; squares show data for profile 75-1R. At distances beyond 24 km, only one time distance value per shot was used for analysis.

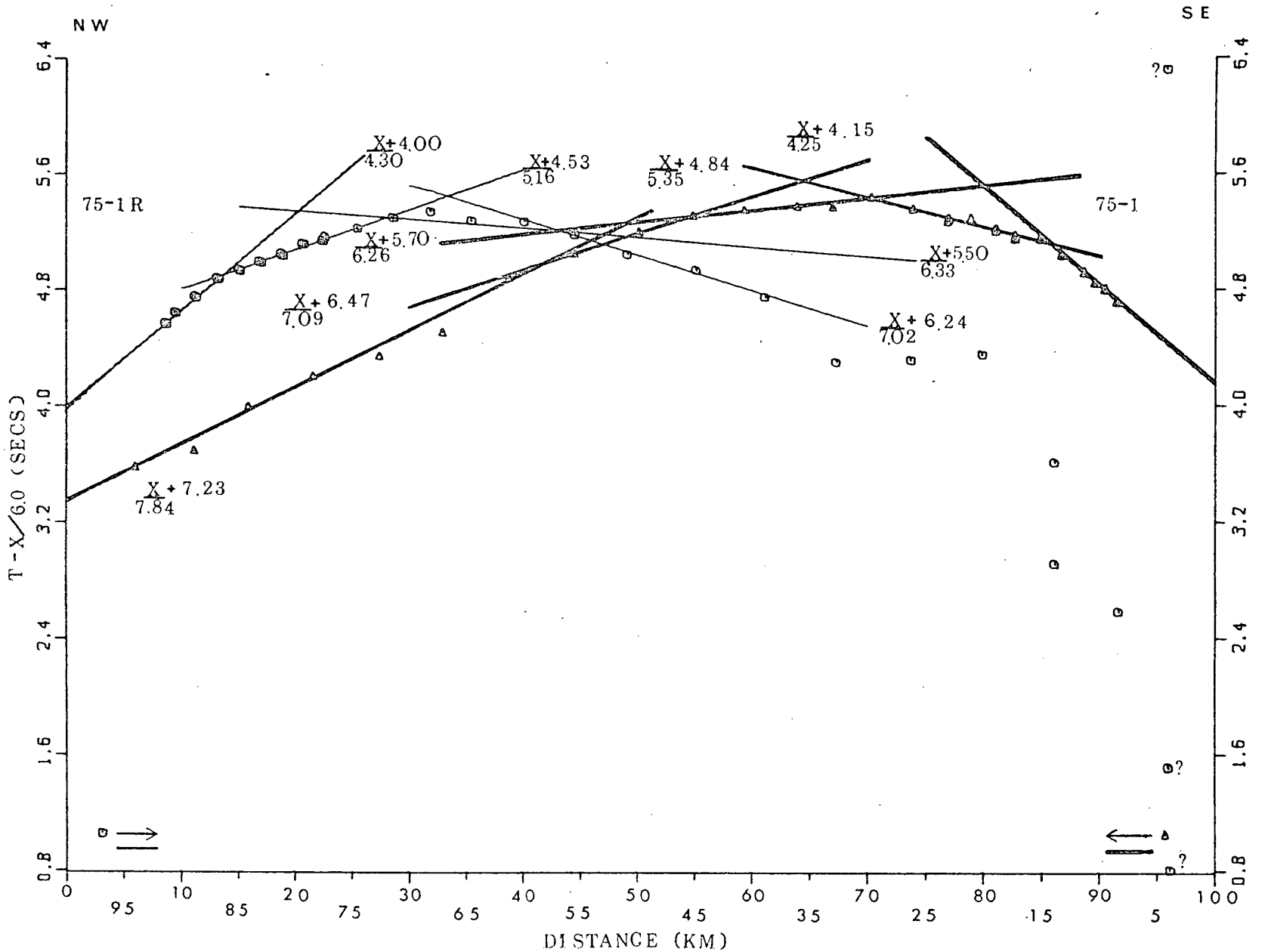
NW
SE
75-1R
75-1
X+4.00
4.30
X+4.53
5.16
X+4.84
5.35
X+4.15
4.25
X+5.70
6.26
X+5.50
6.33
X+6.47
7.09
X+6.24
7.02
X+7.23
7.84
T-X/6.0 (SECS)
DISTANCE (KM)
0
10
20
30
40
50
60
70
80
90
100
95
85
75
65
55
45
35
25
15
5
0.8
1.6
2.4
3.2
4.0
4.8
5.6
6.4

Fig 4.2

Reduced travel time data and least squares fitted lines for the first two phases of profiles 75-1 and 75-1R.

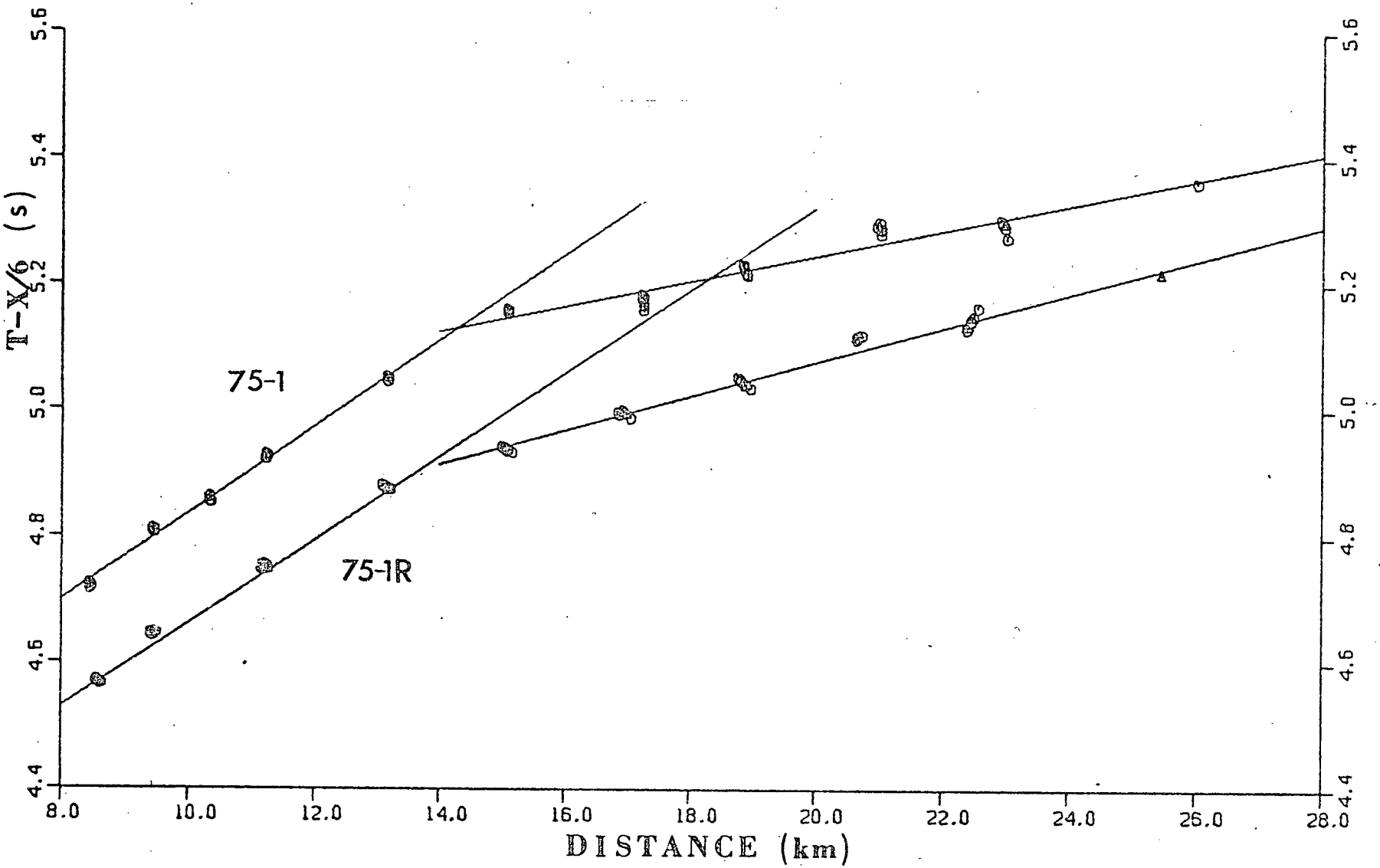
T-X/6 (s)
5.6
5.4
5.2
5.0
4.8
4.6
4.4
75-1
75-1R
8.0
10.0
12.0
14.0
16.0
18.0
20.0
22.0
24.0
26.0
28.0
DISTANCE (km)

only 5 points which is far less than for branches one and two. Travel time branch four with a velocity close to 7.0 km/s becomes the first arrival at about 44 km and remains as such until about 65 km where the 7.8 km/s branch takes over. This arrival, however, is only seen on profile 75-1; the data were too poor to allow it to be seen on profile 75-1R. The reason for the poor data on 75-1R compared with 75-1 probably lies in the fact that the weather during the 75-1R profile was considerably worse, leading to a much poorer signal/noise ratio.

After identifying the first arrival branches, a straight line was fitted to the points using the method of York (1969). His procedure is a least squares technique in which errors in both the X and Y co-ordinates can be considered, in contrast to the usual method that allows only for errors in the Y co-ordinate. The travel time (Y) errors input into the program are the timing errors discussed at the start of this chapter, whereas the distance (X) errors are those associated with the shot-receiver distances discussed in Section 2.4. Fig 4.1 shows the least squares fitted lines superimposed on the first arrival data Table 4.1 gives the least squares slopes, corrected to velocity values, and intercepts, with the associated standard deviations and the number of points defining each line.

There are several methods for obtaining the velocity-depth model from the least squares velocities and intercepts. I decided to use the "Slope Intercept" method of Ewing et al

Table 4.1

Profile	T.T. Branch	No. Pnts.	Velocity (km/s)	Intercept (s)
75-1				
	1	25	4.257 ± 0.010	4.154 ± 0.060
	2	26	5.351 ± 0.005	4.841 ± 0.038
	3	5	6.260 ± 0.020	5.700 ± 0.080
	4	4	7.097 ± 0.007	6.465 ± 0.100
	5	7	7.825 ± 0.040	7.221 ± 0.510
75-1R				
	1	20	4.297 ± 0.009	4.001 ± 0.020
	2	26	5.160 ± 0.005	4.535 ± 0.038
	3	5	6.330 ± 0.015	5.550 ± 0.065
	4	5	7.023 ± 0.010	6.241 ± 0.096

For the first two travel time branches, all traces for each shot were timed; at greater distances only one time-distance value per shot was used.

Table 4.2

Layer	Dip	Velocity (km/s)	Thickness (km) 75-1	75-1R
1	0°	1.49	2.00	2.00
2	0°	2.80[1]	3.03	2.75
3	1.49°	4.28	1.6	1.1
4	-2.35°	5.26	2.74	3.45
5	1.25°	6.28	4.13	3.98
6	0°	7.04	3.76	
7	0°	7.82[2]	?	

1 assumed velocity
2 unreversed velocity

(1939). This method assumes that "each layer is homogeneous and bounded above and below by smooth plane layers and that the seismic velocity in each layer is higher than in the layer above ". This method however does not assume that the layers are flat lying and therefore we can use it to obtain information about the dips on the various refracting horizons.

The velocity depth models generated for profiles 75-1 and 75-1R are shown on Fig 4.3 with the layer velocities and thicknesses given in Table 4.2.

One interesting point concerning these models is the absence of substantial dips of the refracting horizons. For the uppermost layer this is consistent with the continuous seismic profile (C.S.P.) data available for Winona basin. Tiffin et al (1972) and Hopkins (1976) both have C.S.P. lines which show the oceanic basement dipping roughly perpendicular to the direction of profiles 75-1 and 75-1R.

The sediment thickness predicted by this model is roughly 3 km and thus is considerably thicker than the 1.8 km given by the reflection results. This discrepancy is due to the assumption, prior to the analysis of the reflection data, of a 2.8 km/s average velocity for the sediments. As the reflection interpretation section indicates, the average velocity is significantly less than this, accounting for the thinner layer of sediments.

The first point to be made about the model is that all the velocities except the Pn velocity are reversed. This lack of reversal is regrettable especially in the light of the

Fig 4.3

Velocity vs depth models derived from the first arrival analysis. Datum water depth is 2000 m. In this analysis, an average velocity of 2.8 km/s for the sediments was assumed. Subsequent analysis of reflection data (see section 3.2) indicates this is too high.

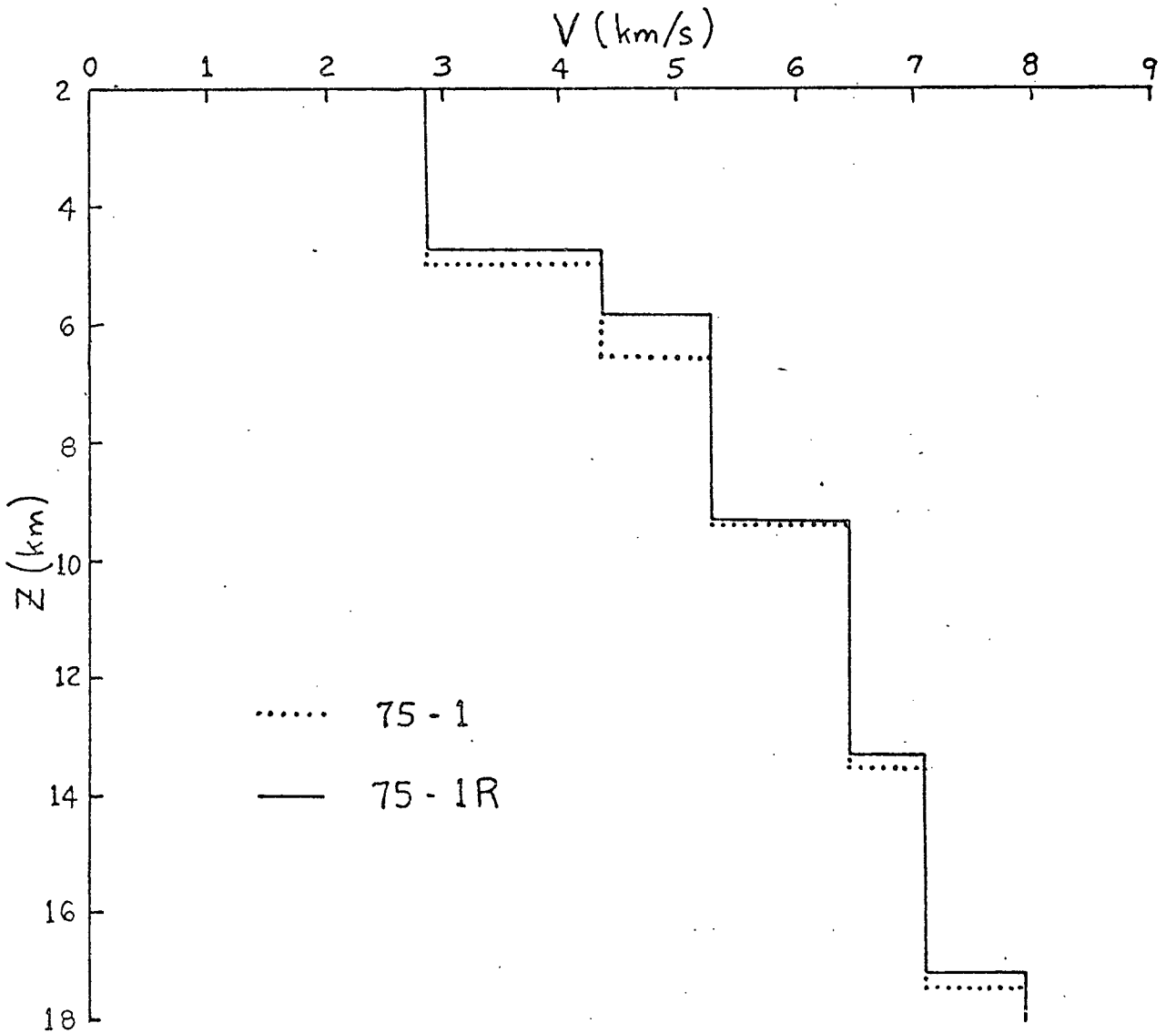
V (km/s)
0
1
2
3
4
5
6
7
8
9
Z (km)
2
4
6
8
10
12
14
16
18
75 - 1
75 - 1R

large relative error (0.040 compared with 0.005 km/s) of this velocity in relation to the other layer velocities.

The first arrival analysis predicts a total sub-bottom thickness of 15 km for the profile with roughly 12 km being sub-sediment (oceanic crust).

4.2 Synthetic Seismograms

Widespread use of synthetic seismograms for interpreting marine seismic refraction data has been implemented only within the last few years. In the past their use has been limited by the expense required for the computations as well as the large amounts of data normally acquired in this type of work. More efficient algorithms and the neccessity of obtaining more detailed information about the oceanic crust has expedited the application of this method. As an example, the establishment of the "Disc Ray Theory" (DRT) concept by Wiggins (1976) has provided a relatively inexpensive and easy-to-use method of calculating synthetic seismograms. Chapman (1976 a,b) has provided the theoretical foundation for the method.

At U.B.C. we are fortunate to have the use of the program HRGLTZ (written by Wiggins), which computes, among other quantities, DRT synthetic seismograms. It has been used both by Malecek (1976) and myself to provide theoretical seismograms for comparison with observed marine refraction data. The algoritm on which HRGLTZ is based calculates travel times and amplitudes for arrivals defined by an input P-Δ

curve. It also performs a Weichert-Herglotz integration of the P-Δ curve to determine the corresponding velocity-depth (V-D) model and includes a modification such that low-velocity layers can be considered.

Whereas we are interested finally in the V-D curve produced by HRGLTZ, it is extremely difficult to use this curve to make changes which reflect the desired changes in the synthetic seismogram sections. This difficulty lies with the interpreter who must propose a change in the V-D curve to provide an expected change in travel time and amplitude of a given arrival. Much more control for this purpose can be obtained by working with the P-Δ curve as indicated by the following two equations.

1) $$T(P,\Delta) = p\Delta + \int_{p}^{p_{max}} \Delta(p)\, dp \qquad 4.2\text{-}1$$

Where $T(p,\Delta)$ = travel time

Pmax=max P value (1/Vsurface)

The travel time, then, can be thought of as the area under the P-Δ curve, presenting us with a simple method of changing the travel time of arrivals (Wiggins and Madrid 1974).

2) $$A(p,\Delta)=F(p,\Delta)\,|dP/d\Delta|^{1/2} \qquad 4.2\text{-}2$$

where $A(p,\Delta)$ = amplitude of the arrival

$F(p,\Delta)$ = a complex function slowly varying with respect to $|dP/d\Delta|^{1/2}$ (Bullen 1963). The last equation states that the amplitude of an arrival is directly proportional to the square root of the slope of the P-Δ curve at that point. Working with the P-Δ curve then allows the interpreter much

more control over the travel times and amplitudes than could be obtained by use of the V-D curve alone.

The inexpensive nature of HRGLTZ and the presence at U.B.C. of an excellent Adage Graphics Terminal allowed the trial of many different models in a short time. The use of the graphics terminal allowed an almost instantaneous comparison between the synthetics and the real data, eliminating the need for expensive computer plots which had a considerably longer turn-around time.

A computer routine named MDLPLT, also written by Wiggins, was used to provide the preliminary P-Δ curve for input into HRGLTZ . This routine approximates a continuous P-Δ curve from an input V-D model according to the equations of Bullen (1963,p112). This program then digitizes the P-Δ curve for future input into HRGLTZ. This digitizing rate (sampling interval) varies over the range of the P-Δ curve, rapidly changing parts of the curve requiring a higher sampling rate than more slowly varying sections.

As often happens, it was not possible to model the real data perfectly. A trade-off between amplitudes, slopes of arrival branches and travel times was necessary since changing one usually affected the others. Greater emphasis was placed on fitting the travel times than on fitting amplitudes, since the travel time determinations were considerably less subjective than amplitude determinations.

4.3 Application to Data

A preliminary V-D model based on the sediment structure from the reflection data for 75-1R (Table 3.2) and the crustal structure from the first arrival analysis of 75-1 (Table 4.2) was used as the starting model for the synthetic calculations. This model was input to MDLPLT in order to obtain the preliminary P-Δ curve, this curve in turn being used as a starting model for 75-1 synthetics. Several problems were encountered with the program MDLPLT, not the least of which was its refusal to output the same V-D model as was input. The degree of matching between the output and input models depended directly on the sampling interval specified for the P-Δ curve. The program uses the input model to calculate an approximate P-Δ curve as specified prevously. It then calls HRGLTZ and produces T-Δ, V-D plots and synthetics. The output V-D model then depends on how finely the P-Δ curve is specified by the initial digitization. This difficulty in getting MDLPLT to generate a P-Δ curve which closely fit the input model made MDLPLT impossible to use for actual modelling. Since only a starting model was required however, this provided no serious problems.

The preliminary P-Δ curve was altered by the famous trial-and-error method, keeping in mind equations 4.2-1 and 4.2-2, to fit the traveltimes amd amplitudes of first and second arrivals for profile 75-1. This final P-Δ curve was then altered further to fit 75-1R. For such calculations it is important to be aware of the difficulties and trade-offs

mentioned previously.

4.4 Record Sections

As a final prelude to the calculation of synthetic seismograms and hence a complete interpretation based on all available information, the refraction data were compiled into record sections as described in section 2.4. Figs 4.4 and 4.5 are the record sections of profiles 75-1 and 75-1R, respectively, for data recorded at distances greater than 6 km. The sections have been corrected for charge size, amplifier gain, spherical spreading and hydrophone sensitivity as described in section 2.4.

These complete profiles are cumbersome to handle computationally. As a consequence, the data were stacked for the purpose of increasing the signal/noise ratio and decreasing the amount of data to be handled. Malecek (1976) has shown that a simple linear stack along a lag trajectory defined by the first arrival velocity was optimum for this type of data. Such a stacking procedure was applied to profile 75-1, the resulting profile being shown on Fig 4.6. Unfortunately, at approximately 35 km on profile 75-1R, the weather conditions deteriorated considerably. This resulted in a decrease in correlation between traces and consequently a large decrease in the stacked amplitudes beyond this distance. Since this was an amplitude variation introduced through processing it made the profile unacceptable. As a compromise a section was compiled using only the data from channel 3, this

Fig 4.4

Record section of profile 75-1 beyond the critical distance for the first crustal refraction arrival. All traces have been amplitude corrected as per section 2.4 and filtered 5.0-30 hz. Prominent secondary arrivals from 2.5 to 10 s after the first arrivals are probably multiples of earlier phases.

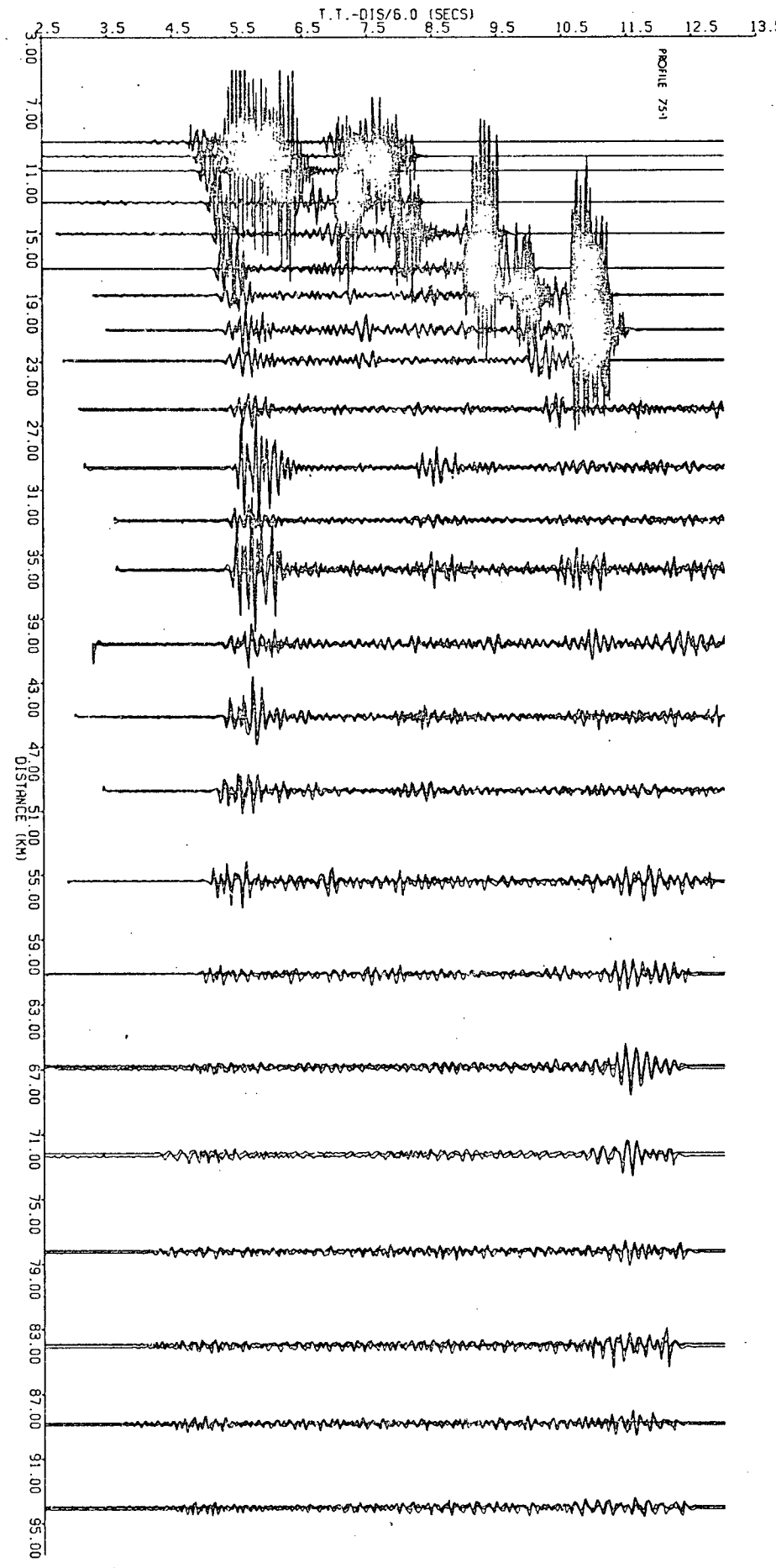
T.T.-DIS/6.0 (SECS)
2.5
3.5
4.5
5.5
6.5
7.5
8.5
9.5
10.5
11.5
12.5
13.5
PROFILE 75-1
DISTANCE (KM)
3.00
7.00
11.00
15.00
19.00
23.00
27.00
31.00
35.00
39.00
43.00
47.00
51.00
55.00
59.00
63.00
67.00
71.00
75.00
79.00
83.00
87.00
91.00
95.00

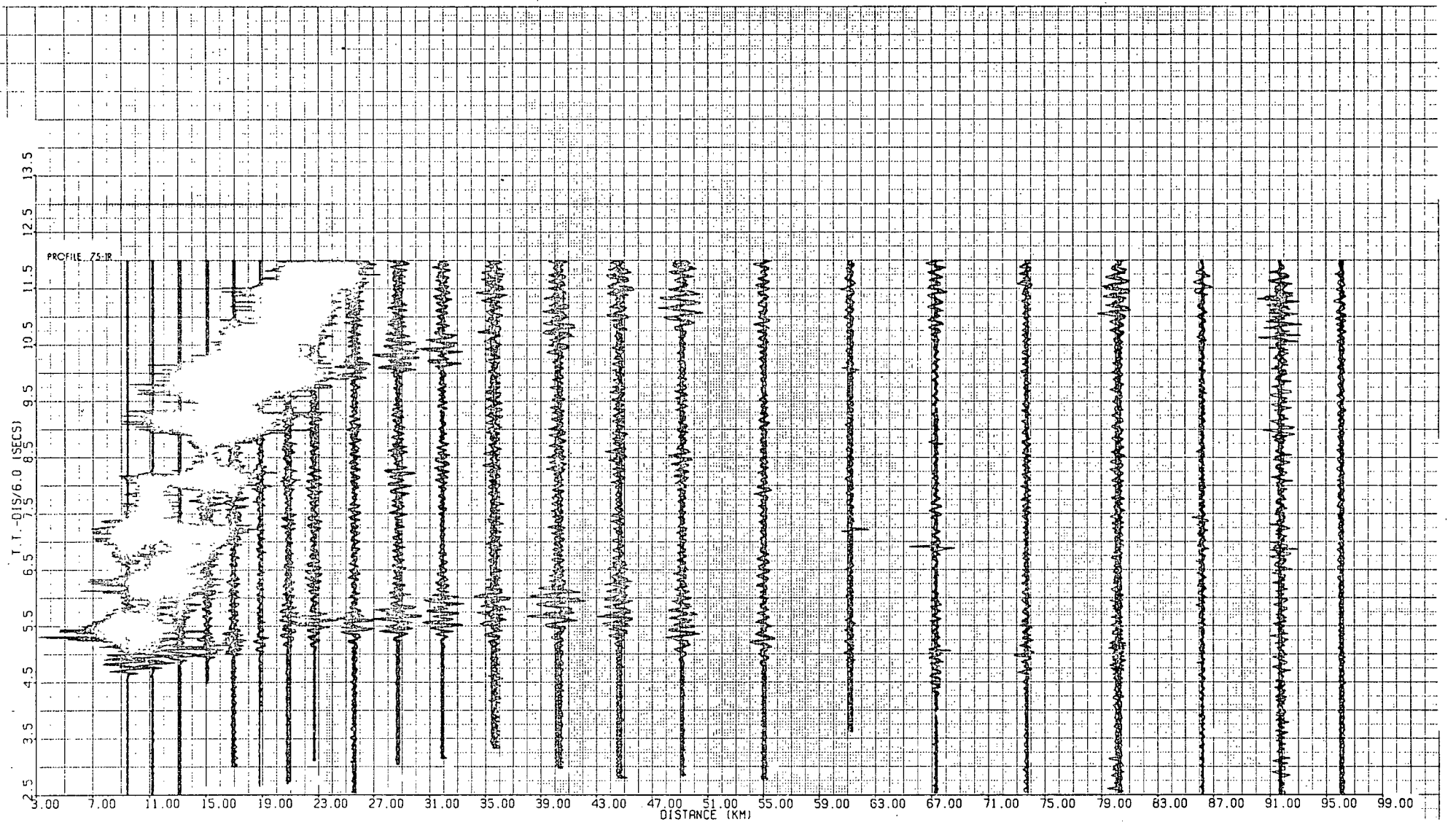

Fig 4.5. Same as Fig 4.4, for profile 75-1R.

Fig 4.6

Record section of data for profile 75-1 after stacking to form a single trace per shot. All traces have been amplitude corrected and filtered 5.0-30 hz. As discussed in the text, an additional amplitude correction was applied to the trace at a distance of 32 km.

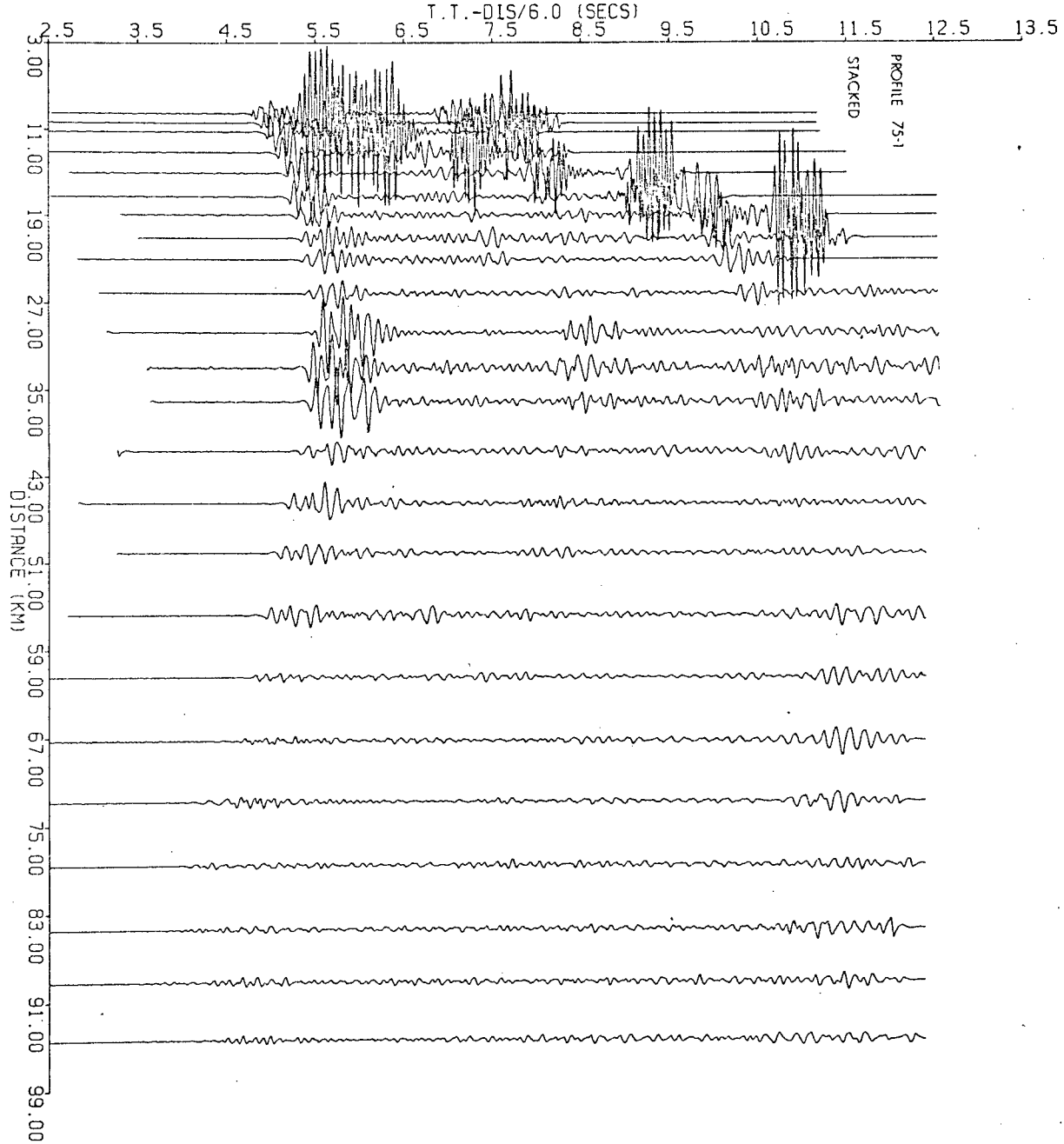
T.T.-DIS/6.0 (SECS)
2.5
3.5
4.5
5.5
6.5
7.5
8.5
9.5
10.5
11.5
12.5
13.5
STACKED
PROFILE 75-1
DISTANCE (KM)
3.00
11.00
19.00
27.00
35.00
43.00
51.00
59.00
67.00
75.00
83.00
91.00
99.00

Fig 4.7

Record section of profile 75-1R channel 3's. All traces have been amplitude corrected and filtered 5.0-30 hz.

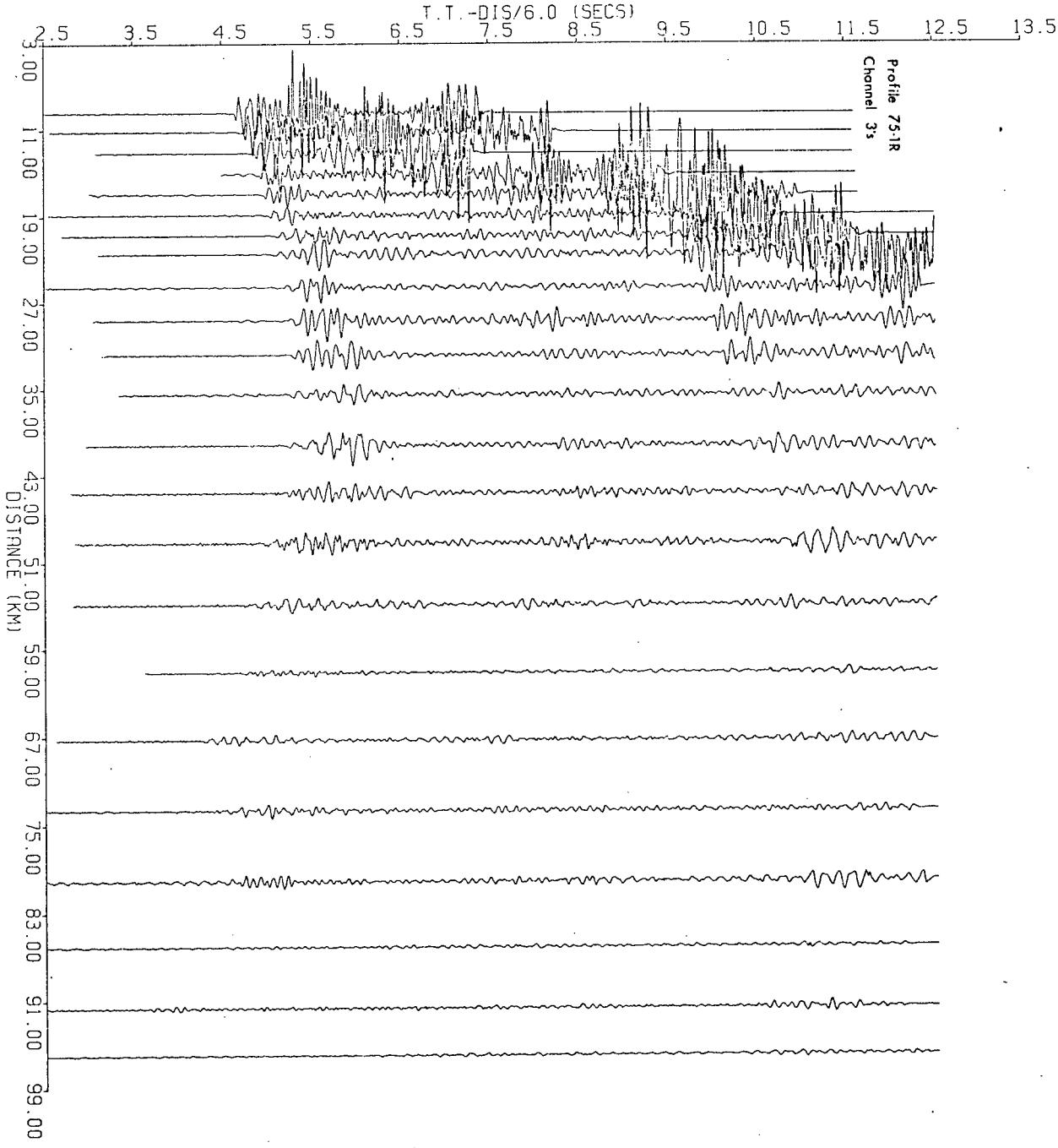
T.T.-DIS/6.0 (SECS)
2.5
3.5
4.5
5.5
6.5
7.5
8.5
9.5
10.5
11.5
12.5
13.5
Profile 75-1R
Channel 3's
DISTANCE (KM)
3.00
11.00
19.00
27.00
35.00
43.00
51.00
59.00
67.00
75.00
83.00
91.00
99.00

channel having particularly good recordings (see Fig 4.7). Whereas this procedure did little to increase the signal/noise ratio, it did allow a considerable saving in data handling and hence computing costs. Although the signal/noise ratio was not improved, for most of the section clear arrivals could still be followed. Both profiles begin with a relatively simple arrival having a substantial amplitude, emerging from the water bottom reflections. This arrival with least squares velocity of 4.28 km/s persists as such for only a short distance. At about 17 km on both profiles, the first arrival becomes much more complex, having about two times the length of the initial first arrival; the amplitude, however, does not change significantly. At about 21 km on both profiles, the first arrivals again appear to increase in complexity, with the amplitude gradually increasing with time along the trace. There also appears to be an overall increase in the amplitude of the arrivals at this point. Between 29 and 36 km on Fig 4.4, we have a series of three arrivals with varying amplitudes. The outside two traces have by far the largest amplitude of any refraction arrivals on either profile, whereas the inner trace has an amplitude consistent with the general amplitude trend of the profile. On the basis of later arrivals it was decided to increase the amplitude of the inner trace to make it consistent with the outer two. This can be seen by comparing Fig 4.4 and 4.6 over the distance range 29-36 km. This was done before the compilation of the 75-1R record sections and before calculating synthetic seismograms.

It appears, however, after studying the sections corresponding to 75-1R and after working with the synthetic calculations, that the inner amplitude should have been left as it was and the outer two amplitudes dropped.

Once again the complexity of the arrival increases at about 29 km on both profiles. The effect of the deteriorating weather during the 75-1R profile can clearly be seen on Fig 4.5 where the background noise level increases considerably at about 35 km.

The amplitude and complexity of the arrivals remain more or less constant out to about 55 km on both profiles. Past this point there is a significant break in the amplitudes of the arrivals on both profiles. At first this was thought to be a processing problem. However, after careful study of later arrivals (11.5 s), it was decided that this sharp amplitude drop was physically real. The length of the arrivals also appear to increase considerably beyond this point, with the majority of the amplitude being due to W.A.R. phases. The first arrival can be followed with little trouble out to the very last shot on profile 75-1, (see Fig 4.6); however it soon becomes lost in the background noise on 75-1R past about 67 km.

Perhaps the most striking feature of both profiles is the lack of secondary arrivals. First and second water bottom multiples can be seen clearly on both profiles at short distances (8.5 s and 10.5 s); however they add nothing to the interpretation and will not be discussed. Fig 4.8 shows the

last 38 km of 75-1 covering all the shots beyond the point at which the amplitudes decrease considerably. The lower profile is filtered 5.0-30 hz and shows both the first arrivals and the W.A.R. energy discussed previously. The upper profile shows the same data filtered 2.0-30 hz. This filtering range reduced the clarity of the first break information but it does show a significant arrival starting at about 6.5 s at a distance of 61 km, and being correlatable along the remaining length of the profile. It is identified as branch f on Fig 4.8. This secondary arrival is a clear indication of the benefit achieved by viewing the data under various filtering limits, as its presence would not have been recognised on the 5.0-30 hz profile alone. The same procedure was tried on the 75-1R data, but the high background noise level and the lack of stacking hindered the processing and no equivalent arrivals could be discerned. An even later secondary arrival that is observable starts at about 40 km on profile 75-1 and is identified by a "?" on Fig 4.11. The amplitude associated with this arrival quickly dies out and at first it does not appear to line up with the continuation of any first arrival or wide angle reflection branch. Its presence, however, did play a role in the synthetic calculations and will be mentioned further in that section.

The two profiles then are remarkably similar with respect to their amplitude structures. Most of the differences in amplitude can be either directly attributed to processing problems or an increase in the ambient noise level between the

Fig 4.8

Expanded plot of the last 40 km of profile 75-1 with the travel time curves of the final model superimposed. Upper section is filtered 2.0 to 15 hz; lower section is filtered 5.0 to 30 hz. Arrows on the lower section give the travel time picks. Note the coherent phases (on the upper section) following travel time branch f.

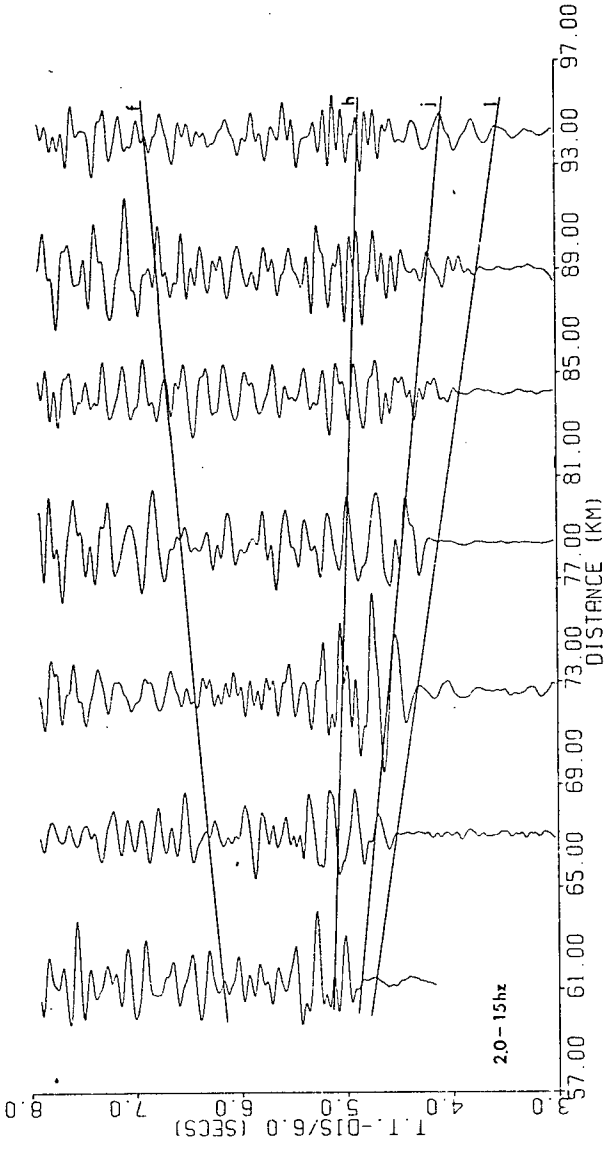
2.0-15hz
T.T.-DIS/6.0 (SECS)
DISTANCE (KM)
57.00
61.00
65.00
69.00
73.00
77.00
81.00
85.00
89.00
93.00
97.00
4.0
5.0
6.0
7.0
8.0

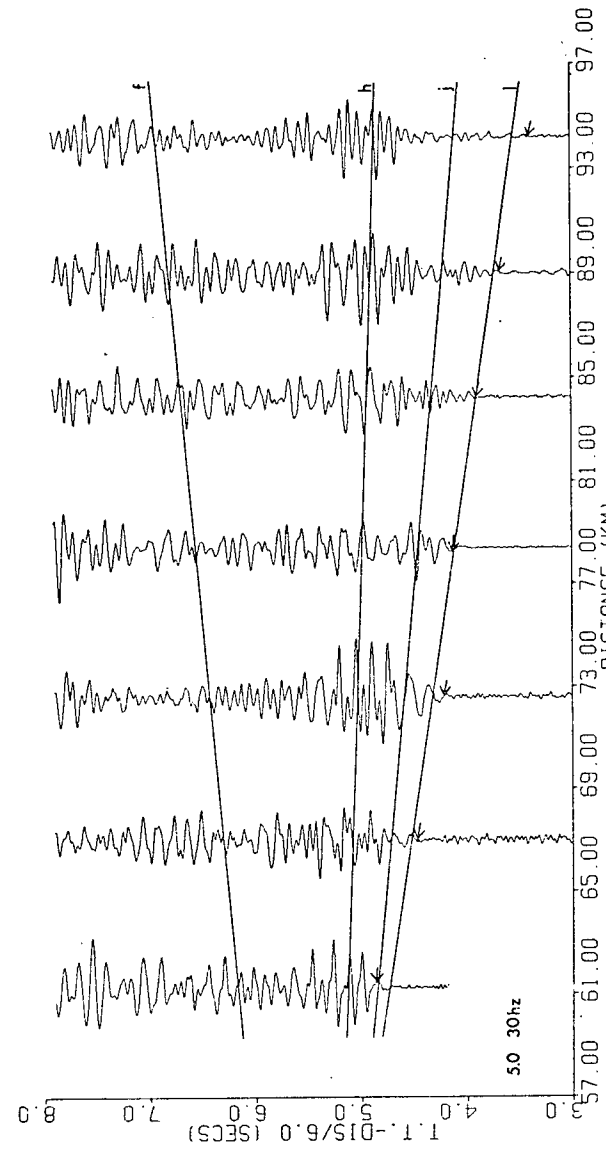
5.0 30hz
T.T.-DIS/6.0 (SECS)
DISTANCE (KM)
57.00
61.00
65.00
69.00
73.00
77.00
81.00
85.00
89.00
93.00
97.00
4.0
5.0
6.0
7.0
8.0

two profiles.

4.5 Comparison of Synthetics with Real Data

As was discussed in section 4.2 the only significant variations between profiles 75-1 and 75-1R is a 200 ms difference in travel times between the two profiles. What amplitude differences there are can be explained either as processing problems, see for example the large amplitudes in the range 27-35 km on 75-1, or as being due to the poorer quality data of profile 75-1R compared with 75-1. For this reason, the fit of the synthetic seismograms to the real data for both profiles will be discussed simultaneously.

The starting P-Δ curve generated by MDLPLT and the corresponding synthetic seismogram section are shown on Figs 4.9 and 4.10. The travel time fit between the starting model and profile 75-1 is extremely close, including possible secondary arrivals, and requires little alteration. The major source of discrepancy between the starting model synthetics and the real data for profile 75-1 is the presence of large W.A.R. phases present on the synthetics. These W.A.R.'s are generated by the discontinuous velocity increases which are given by the first arrival analysis. By far the major effort associated with fitting synthetics to the real data has been in the removal of these W.A.R. phases from the synthetics, while still retaining a reasonable travel time fit. The final synthetic seismogram sections for both profiles, together with the real data are shown on Figs 4.11 and 4.12. The final P-Δ

Fig 4.9

P-Δ curve corresponding to the iso-velocity layered model used as a starting model for calculation of synthetic seismograms for comparison with profile 75-1.

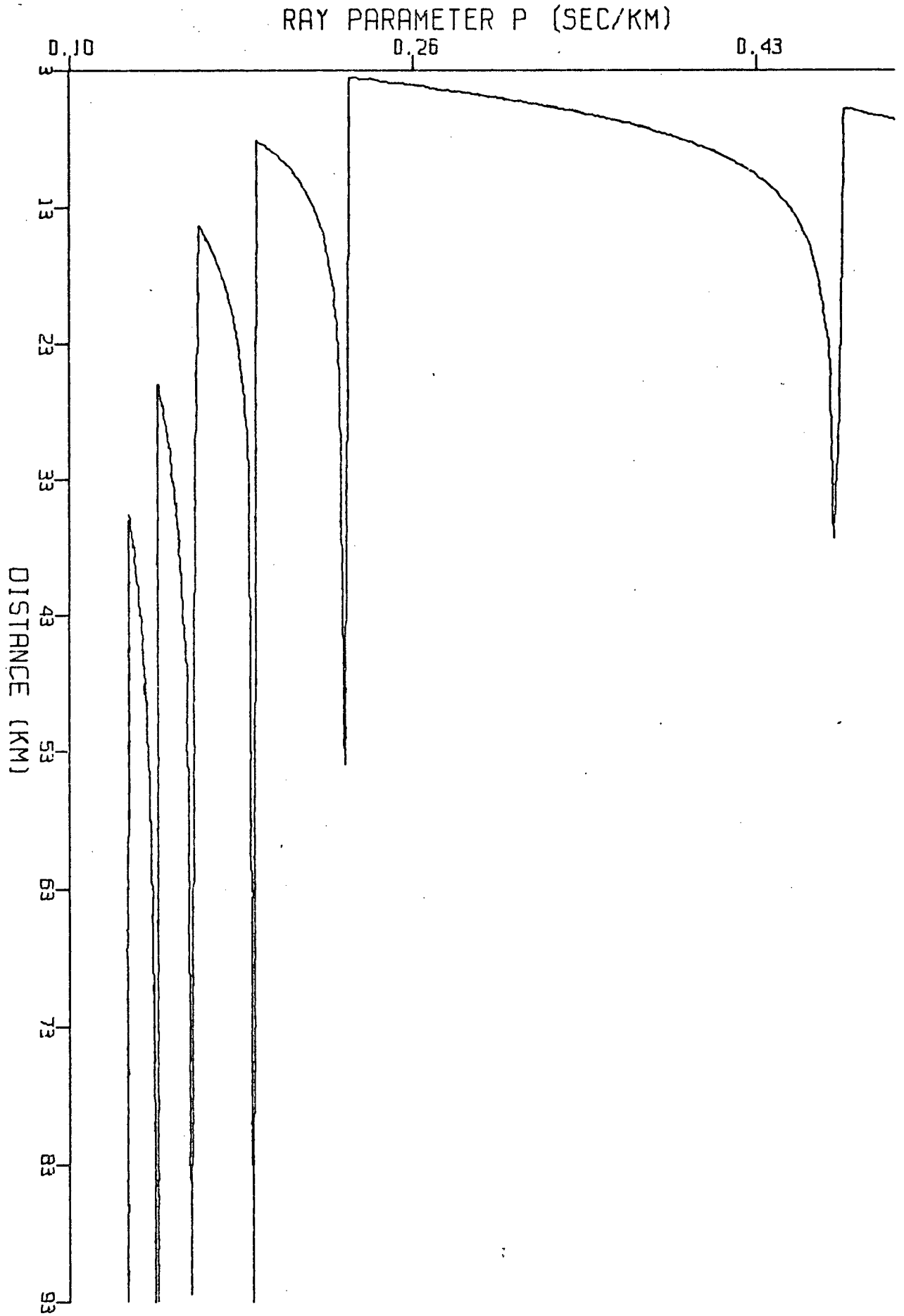
RAY PARAMETER P (SEC/KM)
0.10
0.26
0.43
3
13
23
33
43
53
63
73
83
93
DISTANCE (KM)

Fig 4.10

Synthetic seismogram section for the iso-velocity layered model derived from the reflection data analysis and first arrival refraction data analysis. Note the large amplitudes associated with the wide angle reflections from the velocity discontinuities. Compare with the observed sections of Figs 4.6 and 4.7.

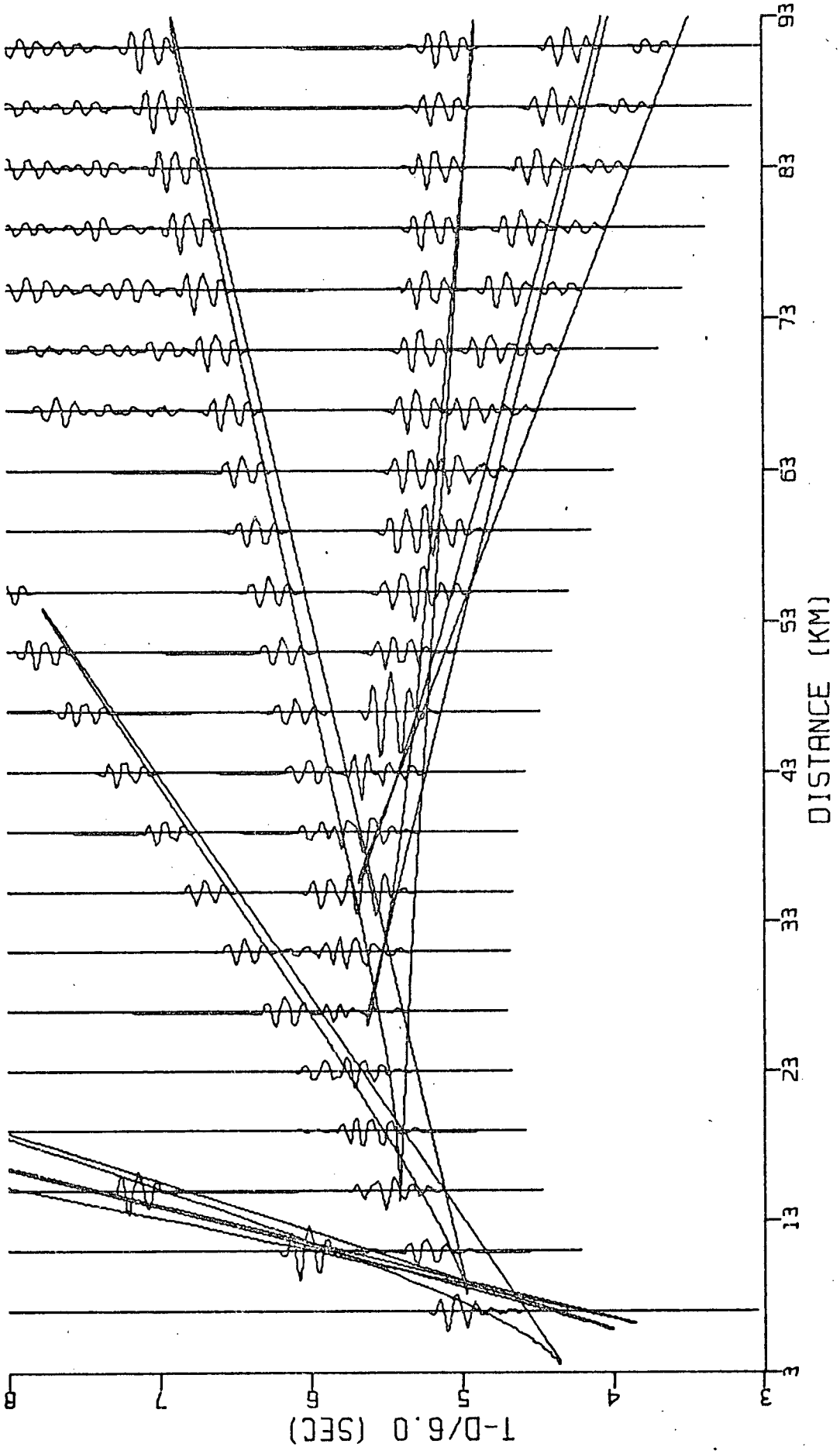
DISTANCE (KM)
3
13
23
33
43
53
63
73
83
93
T-D/6.0 (SEC)
3
4
5
6
7
8

Fig 4.11

Top: Synthetic seismograms and travel times computed to fit the stacked data of profile 75-1. The insert shows the source wavelet which was convolved with the results of the synthetic calculation.

Bottom: Data from profile 75-1 with synthetic travel times superimposed. Lower case letters have been added to identify the various travel time branches. The arrows show the first arrival picks made from the raw data. The phase correlation shown by a "?" seems to line up with the c-d refraction branch.

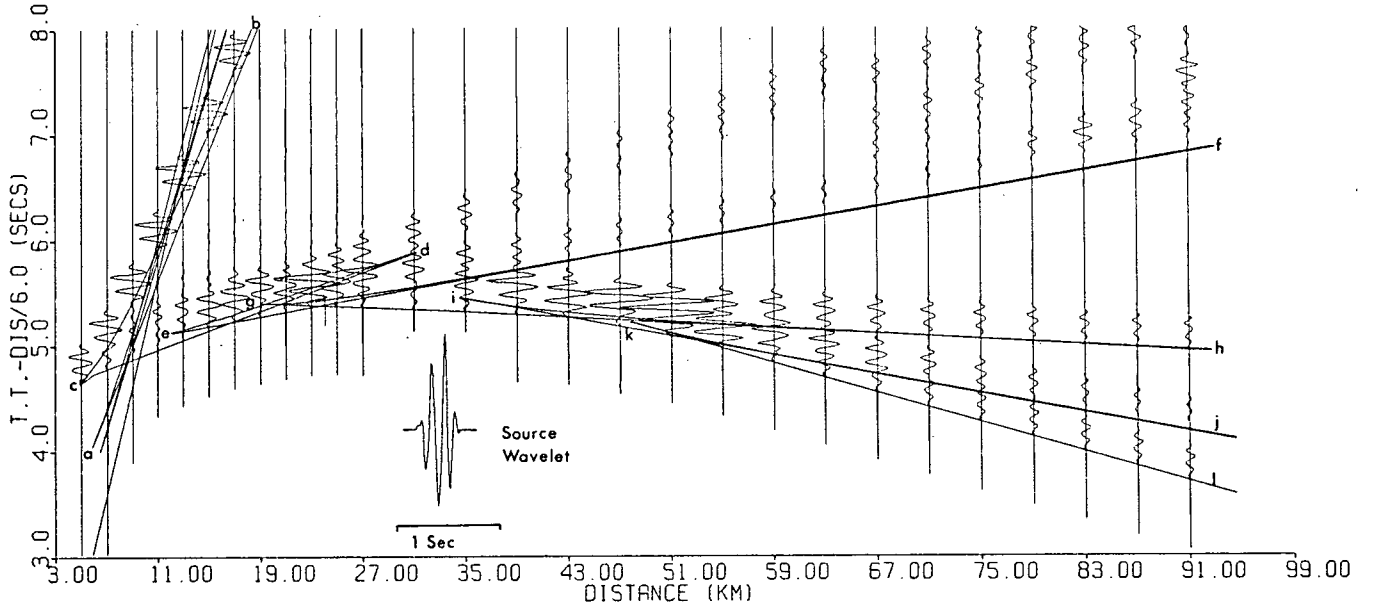
T.T.-DIS/6.0 (SECS)
8.0
7.0
6.0
5.0
4.0
3.0
a
b
c
d
e
f
h
i
j
k
l
Source
Wavelet
1 Sec
3.00
11.00
19.00
27.00
35.00
43.00
51.00
59.00
67.00
75.00
83.00
91.00
99.00
DISTANCE (KM)

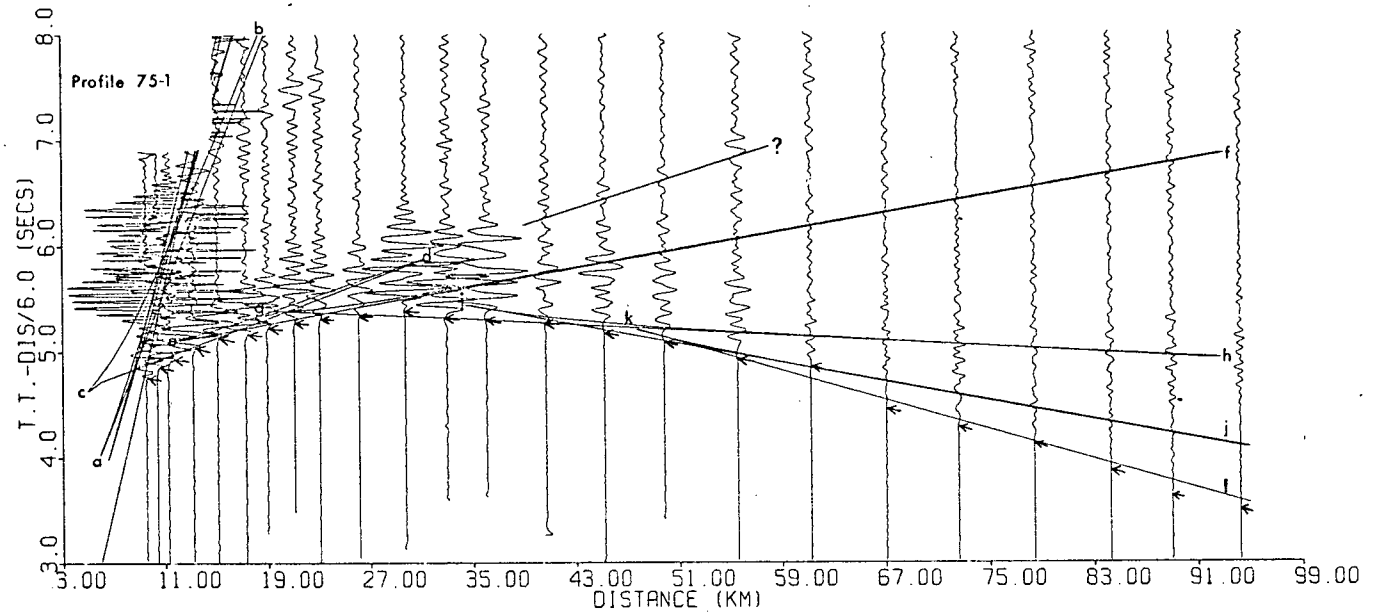
Profile 75-1
T.T.-DIS/6.0 (SECS)
8.0
7.0
6.0
5.0
4.0
3.0
a
b
c
d
e
f
?
h
i
j
k
l
3.00
11.00
19.00
27.00
35.00
43.00
51.00
59.00
67.00
75.00
83.00
91.00
99.00
DISTANCE (KM)

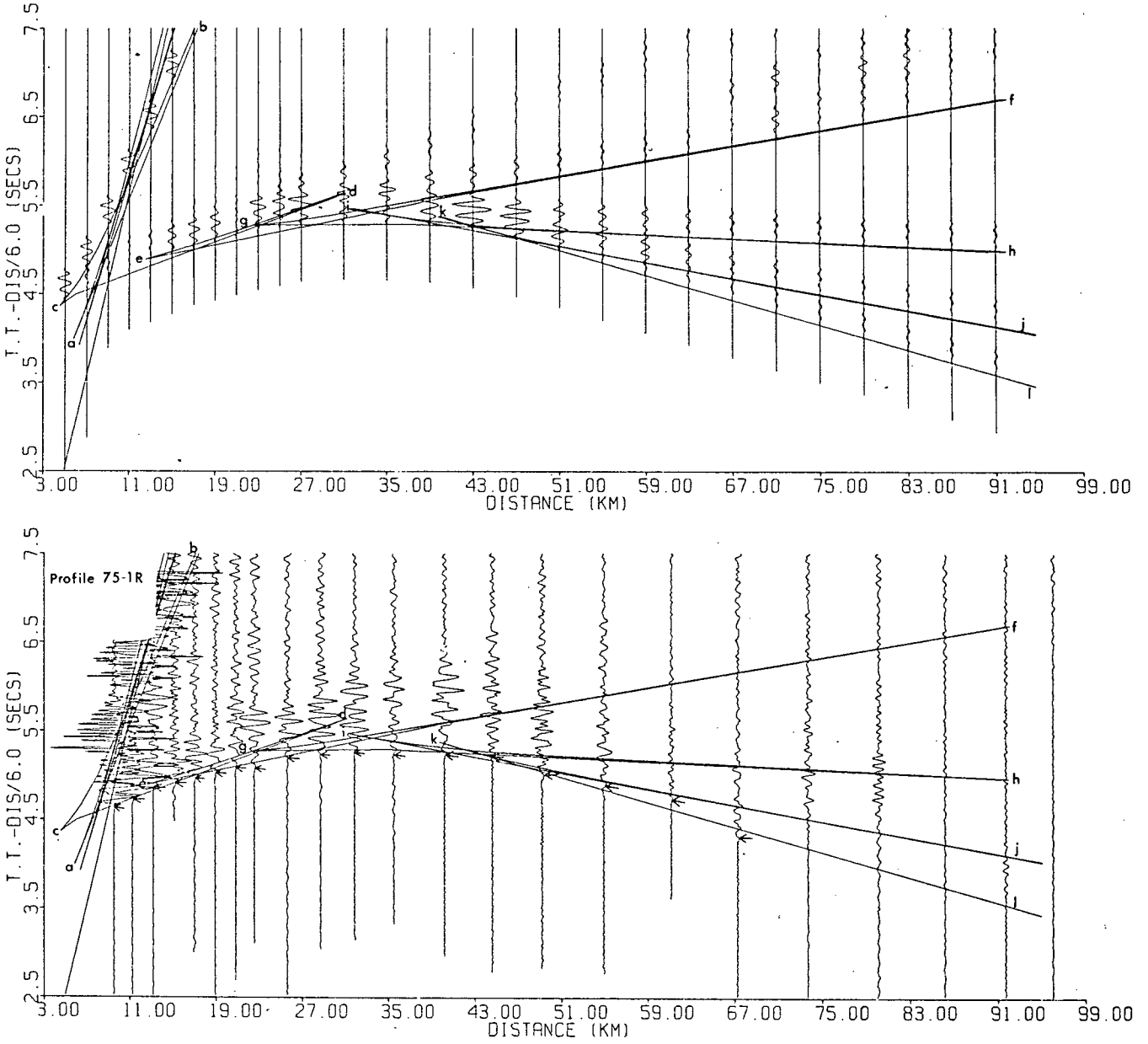

Fig 4.12. Same as Fig 4.11, for profile 75-1R

Fig 4.13

P-Δ curve from which the synthetics for profile 75-1 are computed (Fig 4.11). Starting p-Δ curve (Fig 4.9) is superimposed for comparison.

Fig 4.14

Same as Fig 4.13 for profile 75-1R.

Fig 4.15

Comparison of final p-Δ curves for profiles 75-1 and 75-1R.

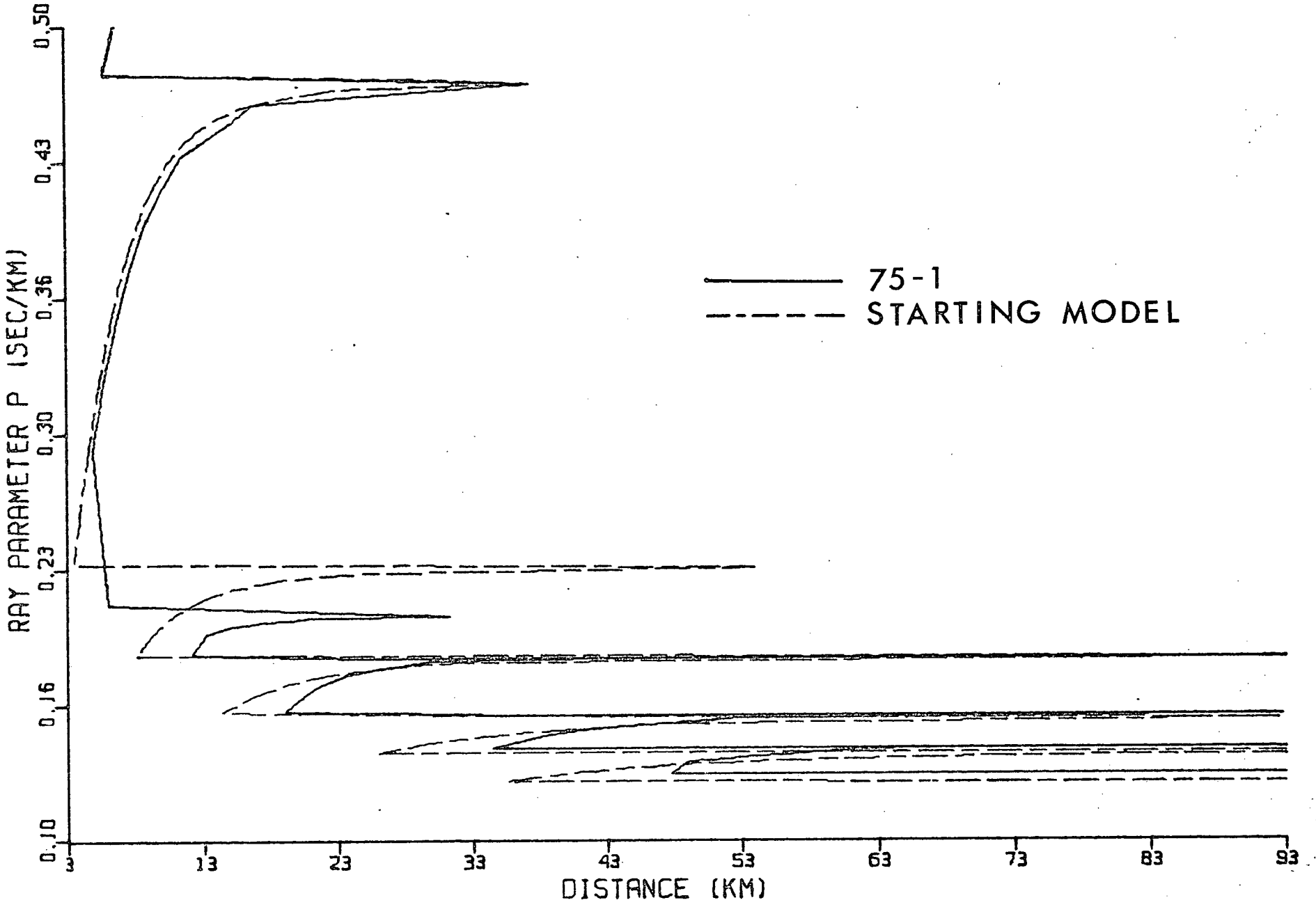
RAY PARAMETER P (SEC/KM)
0.50
0.43
0.36
0.30
0.23
0.16
0.10
3
13
23
33
43
53
63
73
83
93
DISTANCE (KM)
75-1
STARTING MODEL

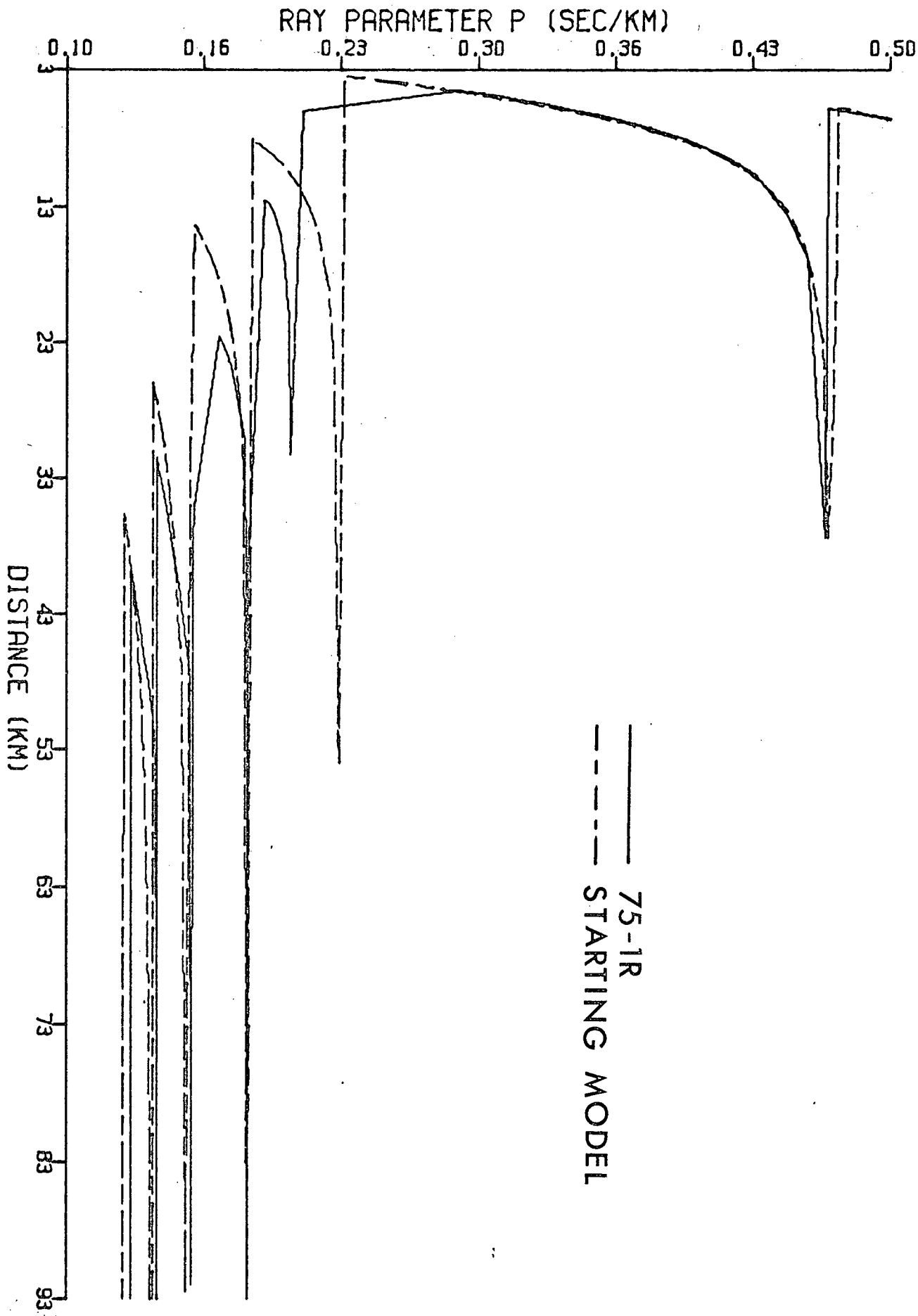
RAY PARAMETER P (SEC/KM)
0.10
0.16
0.23
0.30
0.36
0.43
0.50
3
13
23
33
43
53
63
73
83
93
DISTANCE (KM)
75-1R
STARTING MODEL

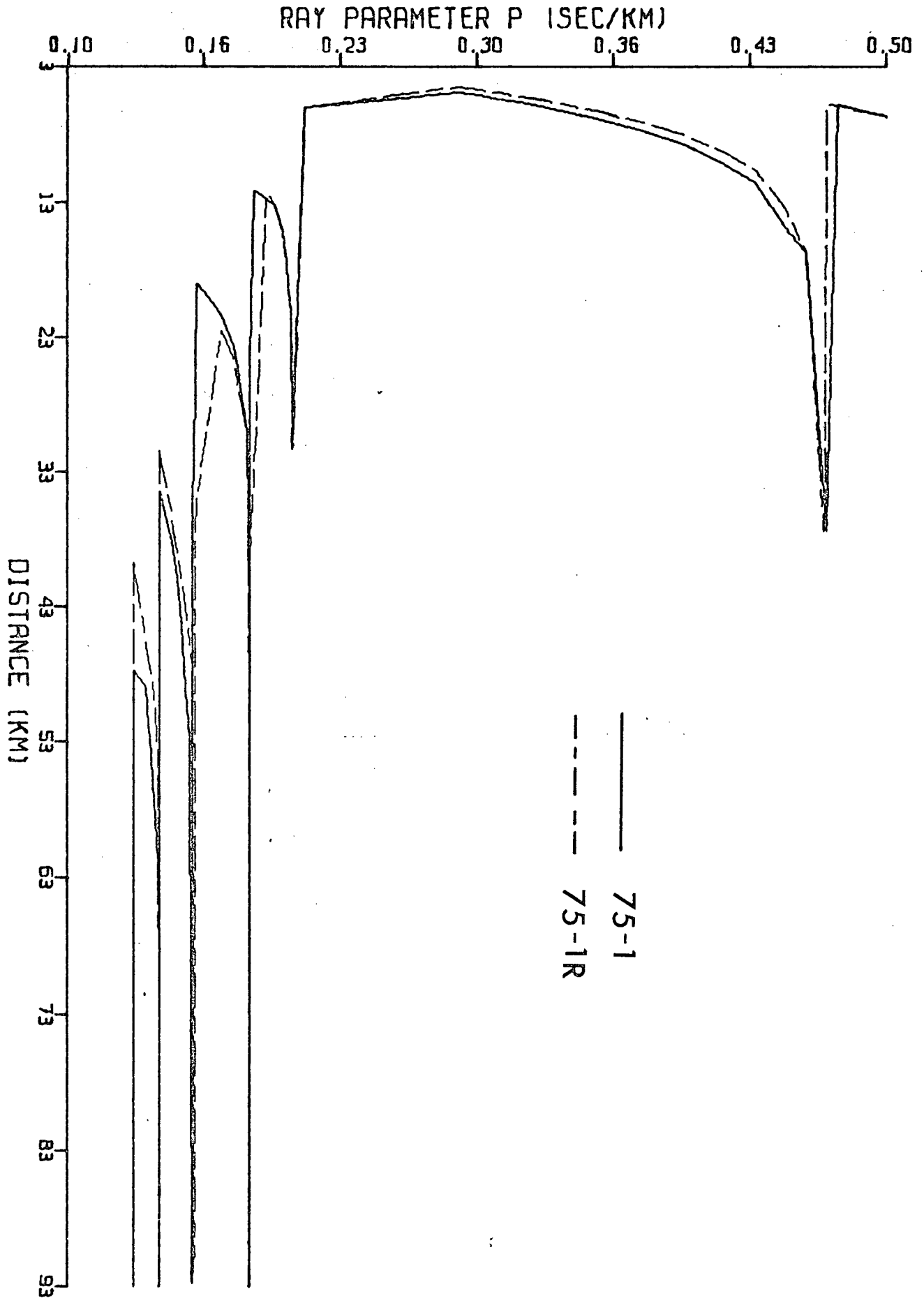
RAY PARAMETER P (SEC/KM)
0.10
0.16
0.23
0.30
0.36
0.43
0.50
3
13
23
33
43
53
63
73
83
93
DISTANCE (KM)
75-1
75-1R

curves are shown on Figs 4.13 and 4.14.

Sediments :

It was not the aim of the synthetic calculations to delineate the sedimentary structure. The sediments are included only to ensure the correct travel time to the first refraction branch (c-d of Figs 4.11 and 4.12). For this reason only the last reflection from the sediments, i.e. the reflection off the top of the oceanic basement , is shown on the synthetic sections (branch b-c). This branch was shown in an effort to calculate the correct amplitude for the first set of refraction arrivals only. It was found that in order to ensure the correct travel times to both the 75-1 and 75-1R first refraction arrivals a difference in the sediment thickness of about 200 m between the two profiles was needed, with 75-1 being the deeper.

Crustal Layers :

As can be seen on Figs 4.4 and 4.5, over the distance range 5-15 km the first refraction branch (c-d) is the first arrival. The amplitudes of these arrivals are quite substantial, being far larger than the corresponding amplitudes generated on the preliminary synthetics of Fig 4.10. I had very little or no success in modelling these large amplitudes on either profile. That this arrival is a head wave can be seen clearly on Fig 3.1 where it can be traced back to the last sub-critical incidence reflection that could be

timed. The fact that this arrival is a pure head wave is significant in that nowhere else on the profiles do we encounter an isolated head wave with any substantial amplitude. The large amplitudes on the sections are due mainly to energy associated with W.A.R.'s; head wave amplitudes are much smaller.

At the start of the modelling, both the slope and travel time of branch c-d agreed very well with the real data. During the process of attempting to generate substantial amplitudes for these arrivals, the slope of the branch was decreased considerably and the travel time fit became much poorer. This is an excellent example of the trade-off mentioned in section 4.3. In order to model the travel times and the slope of this branch correctly I would have been left with no amplitude at all for the arrivals. In an effort to build up these amplitudes, tne fit of the travel times was reduced and the slope of the arrival branch lowered considerably. One interesting point to note is that the secondary arrival identified on Fig 4.6 with a "?" now lines up fairly well with the continuation of this travel time branch. It is possible therefore that this secondary arrival is in some way related to the first refraction/W.A.R. arrival. The correlation between the two though is tentative and the secondary arrival is not seen at all on 75-1R. To conclude then, I do not feel that we can model this first refraction arrival by using the DRT method. The situation is likely to be more complex than we are attempting to model, thus causing the fit between the

synthetics and the real data to be so poor. The reason for this is discussed in section 5.2.

Considerably more success was achieved modelling both travel times and amplitudes for the remainder of the profile. The travel time for the second refraction branch e-f has been fit extremely well. As was mentioned earlier, this arrival is constrained by the presence of W.A.R. energies present to the end of the profile (see Fig 4.8, arrival branch f). The arrivals as well as the model travel time branches are shown on this figure.

The first two W.A.R. branches (d-e, f-g) have been used to generate the increased complexity of the arrivals in the region 15-27 km. As already mentioned, the W.A.R. branch d-e now lines up somewhat with the second arrival shown with a "?" on Fig 4.6. The sudden burst of energy over the range 29-35 km on real profile 75-1 has already been explained as an amplitude over-correction and thus no attempt was made to fit it. Instead I attempted to fit a more or less constant amplitude throughout this region on both profiles. W.A.R. branches f-g and h-i were used to generate the increased complexity of the arrivals over this region with branch f-q being used to stretch out the arrival in time.

It is at this point that the two profiles differ slightly. The travel times between the two were slightly different and to compensate for this I had to move the caustic at positions i and k approximately 7 km further along the profile on 75-1. This allowed me to fit the last two 75-1

travel time branches, i-j and k-l, with considerably more accuracy. This procedure however caused a slight delay in the start of the large amplitudes on profile 75-1 by about 5-7 km, being another example of a trade off between amplitudes and travel times.

The W.A.R. branches h-i, j-k and the refraction branch k-l provide arrival amplitudes for the remainder of the synthetic profiles. They were used to generate the final set of arrival energy over the range 45-95 km. The refraction branches associated with each one have already been discussed and fit the first arrival travel times extremely well. What remains is to see how well the W.A.R. amplitudes fit the real data. There is a significant decrease in amplitudes on the real data at about 61 km. The synthetic sections for both profiles model this as well as can be expected. It is extremely difficult to model sharp amplitude variations and I feel that this has been done as well as the program allows. The amplitudes of the W.A.R. branches h-i and j-k have been fit very well with the amplitudes starting out fairly high at about 55 km and then decreasing until they are just identifiable at the end of the profile.

The final arrival amplitude generated by the refraction branch k-l has not been fit well. Considerable time was spent in trying to decrease the amplitude of this arrival with little or no success. This is most likely a program problem and not physically real. Such a conclusion was reached on the basis of both my own results and the results of Malecek

(1976). His synthetic seismogram sections also show this problem with the final refraction arrival. It would be useful to test whether or not this is a programming problem by either using a different method for computing the synthetics (eg. Generalised Ray Theory; Wiggins and Helmberger 1974), or by artificially introducing a further layer beneath the final layer that generates the Pn arrivals.

The synthetics for the two profiles fit about reasonably well, considering the limitations of the modelling procedure. The procedure assumes horizontal plane layers, a situation that does not hold completely in practice as shown by the slight dips interpreted from the first arrival analysis. The method also does not take into account dispersion or attenuation, lateral variations in the elastic properties of the layers or surface topography; and so it cannot consider the variable nature of the source wavelet due to the lowpass filter effect of the Earth. All of the above are likely to make the arrivals more complex and reverberatory than is allowed for by the modelling procedure.

5 INTERPRETATION AND DISCUSSION

5.1 Velocity-Depth Models

Before attempting to interpret the meaning of the final velocity-depth models produced by the synthetic calculations, it is useful to discuss the significance of the curves produced with respect to the modelling procedure. The final V-D curves are given in Fig 5.1.

The first point to note is that the sedimentary structure shown should not be considered as meaningful in any sense other than in the preservation of the travel time of arrival branch c-d. Not all the sedimentary layers defined by the analysis of reflection profile 75-1R are shown on the diagrams. This is a direct result of the difficulties associated with the program MDLPLT, which was used to generate the starting models for the synthetics. Probably because of the thin sedimentary layers and approximations within the program, it was impossible to generate a V-D model for the sediments that contained all the layers defined in Table 3.2. The only effect of the synthetic calculations has been to deepen the sediments for profile 75-1 by approximately 200 m. This has been done to correct for the approximately 200 ms offset between the travel times of profiles 75-1 and 75-1R. Other than this the synthetics have had no effect on the sedimentary structure.

The layer identified as layer 2a on Fig 5.1 (C)

Fig 5.1

Final velocity vs depth curves for profiles 75-1 and 75-1R determined by fitting both travel times and amplitudes. Also shown is the starting model determined by the travel time fit alone.

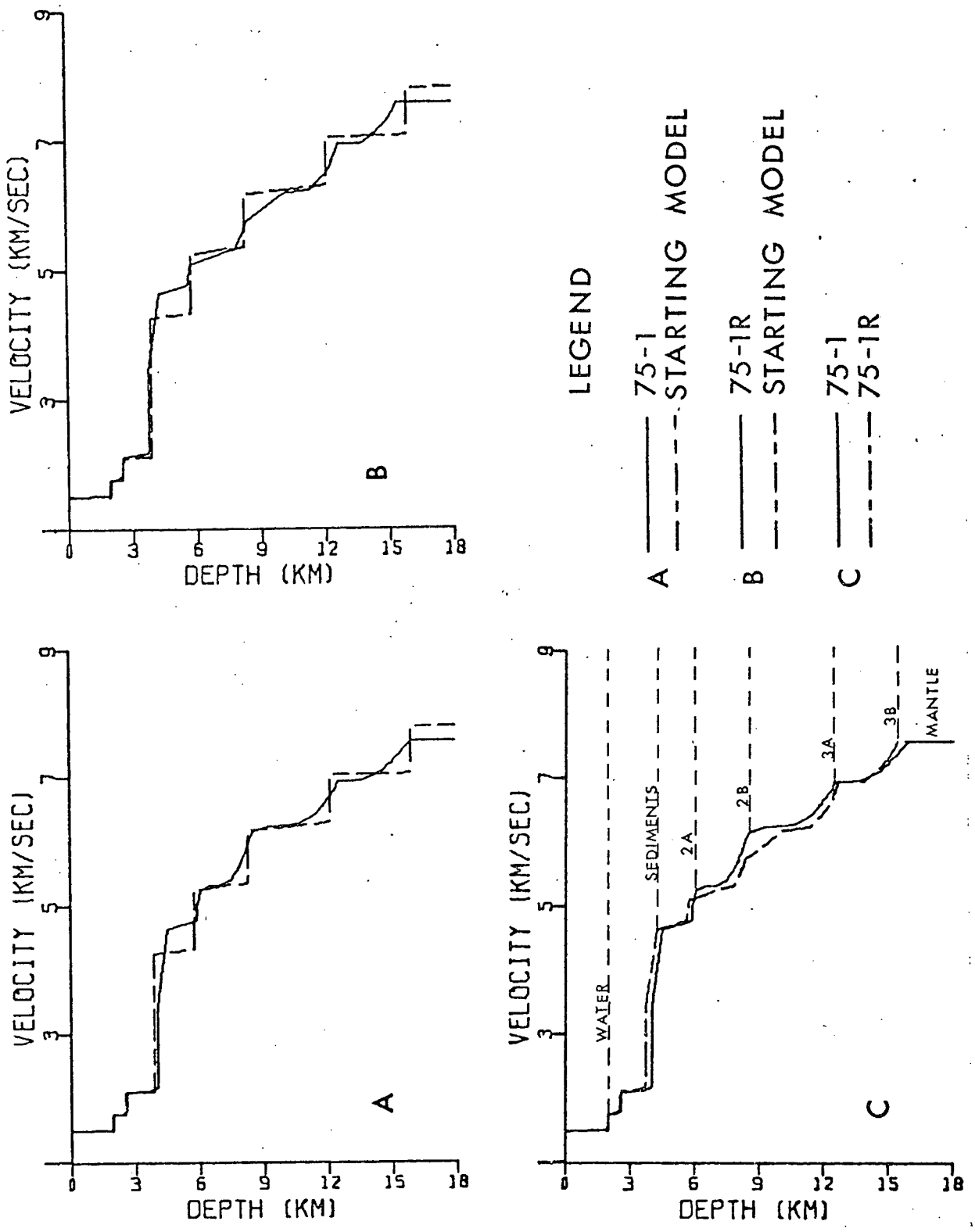
VELOCITY (KM/SEC)
DEPTH (KM)
B
A
C
LEGEND
A 75-1
STARTING MODEL
B 75-1R
STARTING MODEL
C 75-1
75-1R
WATER
SEDIMENTS
2A
2B
3A
3B
MANTLE

represents the transition from the sediments to the basaltic layer. This layer is responsible for the large amplitude refraction arrivals on Fig 4.11 and 4.12, branch c-d. The problems encountered in trying to fit these large amplitudes have previously been discussed in Section 4.5, the conclusion being that the actual structure of this layer is far too complex to be modelled using DRT. For this reason, the V-D curve generated by the synthetics for this layer is no more valid than the first arrival homogeneous layered model.

The remaining three layers, identified as layers 2b, 3a and 3b on Fig 5.1 have been altered significantly by the synthetic calculations. The major change to the curves brought about by the use of the synthetics has been the replacement of the discontinuous velocity increases by smooth gradients. Whereas the gross structure of the V-D curves for each of the three layers is essentially correct, it should be stressed that they are not unique. As a result of the modelling procedure used, it was possible to obtain the same effect on the travel times and amplitudes of the synthetic arrivals by a number of different changes to the p- curves. It is possible that a slightly different V-D curve could have been produced; however, the gross structure of the curves would have remained the same.

The 2b-3a transition differs between the two profiles to a noticeable extent. The actual form of this difference is not overly important. It was introduced to compensate for a slight travel time offset between the profiles. This offset, however,

could have been modelled in several other ways, resulting in slightly different forms for the transition. The important point to note is that the two profiles differ in the nature of this boundary.

Neither the layer depths nor the refraction branch velocities (with the exception of the Pn arrival) have been altered to any great extent by the additional use of amplitude data. The depth to the Moho on profile 75-1R has been reduced by about 500 m, although this should not be regarded as significant since the Pn arrivals on profile 75-1R were not observed. Some depth control for this layer was achieved by manipulating W.A.R. branch j-k; however, the Pn arrival branch is neccessary to define this last refraction branch completely. The lowering of the Pn velocity, observed on Fig 5.1 (A, B), also should not be regarded as significant. It was neccessary to delay this arrival branch (Fig 4.11, branch k-l) by about 100 ms in order to make it agree with the first arrival travel times. In doing this, the 7.8 km/s Pn velocity was reduced to approximately 7.55 km/s. This velocity drop however, is the result of a trade off between travel times, amplitudes near the caustic k and arrival branch slope and is not physically real

To conclude, the V-D curves produced through the use of synthetic seismograms are only valid with respect to the gross structure of the curve and not the fine details. This is not surprising considering that DRT only models thick layers. A recent study by Helmberger (1977) has shown that this type of

approach is only valid in a broad sense and that to delineate the fine structure of the oceanic crust, one must use a large number of very thin layers. The capability to do this does exist at U.B.C. in the form of a computer program called STPSYN which is based on Generalised Ray Theory (GRT), see Wiggins and Helmberger (1974). This type of approach however is considerably more expensive than DRT and beyond the scope of this present project.

The DRT method of calculating synthetic seismograms provides an inexpensive, easy-to-use method of utilising the gross amplitude structure of a refraction profile to delineate the overall velocity-depth structure of the oceanic crust. As such it is an excellent extension of the first arrival method of interpretation. In order however, to delineate the fine structure of a layer, high quality data and the use of GRT is required.

5.2 Discussion

Sediments :

The velocity depth model for the sedimentary structure of the northwest end of the basin (Table 3.2) is a little disappointing. It was hoped that a more detailed picture of the sediments in this area could be obtained. What results we were able to discern however, agree well with the results obtained by Knize (1976) for two short profiles in the area between J. Tuzo Wilson Knolls and the Queen Charlotte Sound,

about 60 km north of the receiving ship location for profile 75-1R. His interpretation includes a series of alternating high and low velocity sedimentary layers, with a thickness of roughly 300 m each. The total sedimentary thickness in this area is approximately 2 km, very close to the depth of the sediments in Winona Basin. He interpreted the sedimentary sequences as being due to alternating periods of glacial (low velocity coarse sediments) and inter-glacial (high velocity fine sediments) deposition. Although the results in Winona Basin do not show the same detail, due to poorer quality data, the upper two layers are both roughly 300 m thick and have velocities consistent with those found by Knize.

At the southern end of Winona Basin the same reflecting horizons can be identified as at the northern end, although they are considerably more folded with dips ranging from $+10^{o}$ to -10^{o}. Considering then the close proximity of Winona Basin to the sedimentary area studied by Knize, and considering that the same reflectors can be identified at both ends of the basin, it is reasonable to assume that the depositional history of Winona Basin may be similar to that of the area to the north discussed by Knize (1976).

Even though it was hoped to obtain a detailed picture of the sedimentary structure within the basin, the main objective was to obtain a more accurate depth for the sediments than has previously been reported (Tiffin 1973, Couch 1969). To this extent, the study was a success. The total sedimentary thickness for the sediments in Winona Basin has been found to

be approximately 2 km. This value differs greatly from the 4 to 6 km previously suggested by the afore mentioned authors. The previous studies, however, have based their depths on gravity data, the lack of an observable basement on C.S.P. lines, and on an assumed velocity structure used to convert the C.S.P. travel times into depths. However, the C.S.P. lines for the area penetrated only to a maximum of about 4 s 2-way travel time (Figs 1.3 to 1.5). Thus they were only about 0.5 seconds from the actual basement, which can be seen at about 4.5 s on reflection profiles 3.1 and 3.2. On the basis of good reflection and refraction data, it is believed that a sediment depth of 2 km is a better interpretation than the previously reported depths of 4 to 6 km.

Basement layer :

The transition from sedimentary material to basaltic basement is represented by layer 2a on Fig 5.1. This layer has a least squares velocity of 4.28 km/s which is compatible with the velocity given by Peterson et al (1974) for layer 2a The observation of a 4.28 km/s velocity for the first basaltic layer is not unique in the region. Similar results have been found by Malecek (1976) for the oceanic basement layer in the region of Explorer Ridge where there were less than 250 m of sediments. He obtained velocities in the range 4.06-4.20 km/s and thicknesses of 0.97-1.71 km/s for his profiles parallel and perpendicular to Explorer Ridge. Knize (1976) has also obtained similar results in two areas. In the area between J.

Tuzo Wison Knolls and the Queen Charlotte Sound he found a transition layer with velocity 4.2 km/s and sub-bottom depth 2.2 km. Further, in the region of northern Cascadia basin about 200 km east of Winona Basin, he found that the transition layer consisted of a series of three layers with velocities of 4.56, 3.78 and 4.43 km/s and thicknesses of 0.41, 0.40 and 1.5 km respectively, stacked on each other beginning at a sub-bottom depth of 2 km.

As has already been mentioned, the large amplitude arrivals from this layer have not been fit synthetically (section 4.5). This fact leads us to the conclusion that a simple velocity structure is not sufficient to explain the results. A recent study over the Mid-Atlantic Ridge by Hyndman et al (1976) could possibly shed some light on the reasons for this. On the basis of drill cores penetrating layer 2a they have found that it consists of highly porous, low density, fractured volcanic material with some intercalated sediments. These results illustrate that this layer is characterised by a mixture of fractured volcanic material and low velocity sediments. While the Winona Basin in no way resembles the Mid-Atlantic Ridge, the results of Hyndman et al do show the highly inhomogeneous nature of this transition layer. It would not be unreasonable to assume that if Winona Basin were created while the sediments from the nearby continent were being deposited, the transition layer between the sediments and basement would be a mixture of high and low velocity basalts and sediments. This in fact has been postulated by

Knize for his results in the northern Cascadia basin. His reflection results for the area showed a low velocity sediment/basalt layer (3.78 km/s 0.4 km) sandwiched between two higher velocity basaltic layers (4.56 km/s, 0.41 km thick; 4.43 km/s, 1.5 km thick) Such fine layering however, could not be delineated by the longer wavelength signals recorded during the refraction part of his profiles.

If this layer is a complex mixture of high and low velocity materials, then the large amplitude signals could be explained as being due to either a focussing or constructive interference effect. In any event the DRT modelling procedure is too simple to explain the velocity-depth structure of this layer. It is hoped that after further processing of the reflection data, eg. w-k filtering (section 3.1), the complex nature of this layer can be further revealed.

Lower Crustal Layers :

The least squares velocites and depths of the remaining three layers are listed in Table 4.1. These have velocities consistent with layers 2b, 3a, and 3b, respectively and have been identified as such. All of the sub-basement layer depths are close to the maximum values reported for a standard oceanic section (Peterson et al 1974). However, the total sub-sediment crustal thickness of 12 km is considerably thicker than the 5 to 7 km normally considered standard for an oceanic crust.

The velocity gradients introduced into the V-D models by

the synthetics have already been discussed somewhat. What remains however is to discuss the significance of the gross structure of the curves. The curves produced for layers 2b, 3a, 3b are all similar. They indicate a gradual transition from one layer to the next caused either by compaction or intermixing of the adjacent layers or both. Once the transition from one layer to the next is complete however, the velocity remains nearly uniform with depth for the next 2-3 km (with a slight positive gradient). On the basis of these curves, it appears that the lower crust in this region is strongly divided into three separate layers, possibly reflecting different rock types under different pressure-temperature conditions in each layer.

As interpreted in this study, the crust underlying Winona Basin has a typical oceanic velocity structure but is considerably thicker than what is normal. In the region of Explorer Ridge, Malecek (1976) has found similar thicknesses to those observed underlying Winona Basin. His reversed profile (74-2,2R) crossing Explorer Ridge show a sub-bottom depth to the mantle of 9 to 11 km. Considering that the sediment cover in this region is minimal, these results agree well with the 12 km sub-sediment crustal thickness underlying Winona Basin. A detailed examination of his data reveals that they are remarkably similar to those observed on profiles 75-1 and 75-1R with respect to both travel times and amplitude information. On the basis of this, and the similarity between the velocity vs depth models interpreted for Winona Basin and

Explorer plate just east of the spreading centre, it would seem that the crust in the two regions was formed in much the same manner.

The thick crust, then, does not seem to be localized only beneath Winona Basin. In fact an OBS study of the crustal structure beneath Juan de Fuca Ridge, (Davis et al 1976) has shown a similar crust with a thickness of 10-11 km sub-sediment. Whereas these data are not of the same quality as those used by Malecek (1976) or in this study, it does indicate that the thick crust is a widespread feature.

A preliminary interpretation of a reversed refraction line recorded parallel to and south of the Revere-Dellwood fracture zone and west of northern Explorer Ridge (Fig 1.1) has indicated that the crust in this region is similar to a standard oceanic section (R.D. Hyndman personal communication 1977). These results are tentative however because of the lack of observable Pn arrivals on the analog playbacks. If this is the case though, the crustal thickness changes drastically as one crosses both Explorer Ridge and Paul Revere Ridge. This change in thickness could be a direct result of the differing tectonics of the opposite sides of the ridges. The Explorer plate, having a thick crust, is trapped between the North American, Pacific and Juan de Fuca plates. As a result, its movement away from the spreading centre could be restricted causing a piling up of the newly formed oceanic material. This idea has been suggested by Malecek and Clowes (1977) as one possible explanation for the thick crust in the region of

Explorer Ridge. On the other hand, the movement of the Pacific plate is unrestricted and hence this piling up effect should not be observed.

If Winona Basin was created at the time Explorer Ridge terminated at the Brooks fracture zone, and was subsequently isolated by rotation of the plate, then we would expect it to have the same type of crust as the Pacific plate to the northwest of the present Explorer Ridge. This is not the case. The basin has a thicker crust than the Pacific plate, the implication being that it has not been created by spreading from Explorer ridge. This tends to refute a possible argument that Winona Basin is an isolated section of old Pacific material.

A more reasonable suggestion is that Winona Basin has been created by the slow northward movement of the triple point. The spreading rate in the basin would most likely be extremely slow due to it being trapped between the spreading centre (Dellwood Knolls) and Brooks fracture zone. The thick crust underlying Winona Basin then could be formed by a piling up of the new crustal material, in much the same way as postulated for the crust beneath Explorer plate.

The lack of any significant magnetic anomaly pattern in the basin has already been mentioned in Chapter 1. If Winona Basin has been formed in the last 3-4 my, by the movement of the triple point, then what has happened to the magnetic anomalies ? This is a difficult question to answer. Perhaps it is possible that if the spreading centre creating the basin

were very diffuse, and if the spreading were extremely slow, no discernible anomaly pattern would be created.

The thick crustal section, including only 2 km of sediments, implies that a reconsideration of the gravity data (Couch 1969) is required. A thick crust is consistent with the -160 mgal free air anomaly, as shown by Couch, but the lack of a thick sediment pile will require other changes in his model. Also, the gravity low tends to terminate at Winona Ridge rather than Paul-Revere Ridge. What does this mean in terms of crustal structure ? Such a question lends added importance to the analysis, currently in progress, of the two reversed DSS profiles across the basin.

The explanation given here of the origin of the thick crust interpreted from the seismic profiles along Winona Basin is, of course, highly speculative. Subsequent analysis of the remaining two reversed DSS profiles in Winona Basin, more detailed analysis of the OBS data to the west of Explorer Ridge, and additional geophysical studies in progress will hopefully provide more evidence to aid in fully understanding this complex and fascinating area.

T.A.F.

REFERENCES

Atwater, T. 1970. Implications of plate tectonics for the Cenozoic tectonic evolution of western North America. Geol. Soc. Am. Bull. 81, pp. 3513-3536.

Barr, S.M. and R.L. Chase 1974. Geology of the northern end of Juan de Fuca Ridge and sea-floor spreading. Can. J. Earth Sci. 11, pp. 1384-1406.

Bertrand, W.G. 1972. A geological reconnaissance of the Dellwood Seamount area, northeast Pacific Ocean, and its relationship to plate tectonics, Unpublished M.Sc. thesis, University of British Columbia.

Braille, L.W. and R.B. Smith 1975. Guide to the interpretation of crustal refraction profiles. Geophys. J.R. astr. Soc. 40, pp. 145-176.

Bullen, K.E. 1963. An Introduction to the Theory of Seismology, 3rd ed., Cambridge University Press, New York, 381 pp.

Cerveny, V. and R. Ravindra 1971. Theory of Seismic Head Waves, University of Toronto Press, 312 pp.

Chapman, C.H. 1976a. A first-motion alternative to geometrical ray theory. Geophys. Res. Lett. 3, pp. 153-156.

_____, 1976b. Exact and approximate generalised ray theory in vertically inhomogeneous media. Geophys. J.R. astr. Soc. 46, pp. 201-233..

Chase, R.L., D.L. Tiffin and J.W. Murray 1975 The western Canadian continental margin. Canadian Society of Petroleum Geologists, Memoir 4, pp. 701-721.

Clowes, R.M. 1977. A Marine deep seismic sounding system. Can. J. Earth Sci. 14 (in press).

Couch, R.W. 1969. Gravity and structures of the crust and subcrust in the northeast Pacific ocean west of Washington and British Columbia. Unpublished PhD thesis. Oregon State University, Corvallis, OR.

Davis, E.E., C.R.B. Lister, and B.T.R. Lewis 1976. Seismic structure on Juan de Fuca Ridge: ocean bottom seismometer results from the median valley. J. Geophys. Res. 81, pp. 3541-3555.

Dix, C.H. 1955. Seismic velocities from surface measurements.

Geophysics 20, pp. 68-86.

Ewing, M., G.P. Woollard and A.C. Vine 1939. Geophysical investigations in the emerged and submerged Atlantic coastal plain, Part III: Barnegat Bay, New Jersey section. Geol. Soc. Amer. Bull. 50, pp. 257-296.

Helmberger, D.V. 1977. Fine structure of an Aleutian crustal section. Geophys. J.R. astr. Soc. 48, pp. 81-90.

Hopkins, N. 1976. The continuous seismic profile technique with an application to Winona Basin. Unpublished B.Sc. thesis University of British Columbia.

Hyndman, R.D., F. Aumento, W.G. Melson, J.M. Hall, H. Bougault, L. Dmitriev, J.F. Fisher, M. Flower, R.C. Howe, G.A. Miles, P.T. Robinson and T.L. Wright 1976. Seismic structure of the oceanic crust from deep drilling on the Mid-Atlantic Ridge. Geophys. Res. Lets. v 3, pp. 201-204.

Kanasewich, E.R. 1976. Time Series Analysis in Geophysics, University of Alberta Press, 352 pp.

Keen, M.J.. The ray parameter method for the reduction of wide-angle reflection data. Unpublished report, Dalhousie University.

Knize, S. 1976. Marine deep seismic sounding off the coast of British Columbia. Unpublished PhD. thesis, University of British Columbia.

Malecek, S.J. 1976. A marine deep seismic sounding survey in the region of Explorer Ridge. Unpublished M.Sc. thesis, University of British Columbia.

_____, and .R.M. Clowes 1977. Crustal structure near Explorer Ridge from a deep seismic sounding survey. Submitted to J. Geophys. Res..

Milne, W.G., G.C. Rogers, R.P. Riddihough, R.D. Hyndman and G.A. McMechan 1977. Seismicity of western Canada (preprint; to be submitted for publication in Can. J. Earth Sci.).

Mueller, St., A. Stein and R. Veis 1962. Seismic scaling laws for explosions on a lake bottom. Zeit. f. Geophys. 28, pp. 258-280.

Murray, J.W. and D.L. Tiffin 1974. Patterns of deformation sedimentation and tectonism southwestern Canadian continental margin. Annales de la Societe Geologique de Belgique. 97, pp. 169-183.

O'Brien, P.N.S. 1960. Seismic energy from explosions. Geophys.

J.R. astr. Soc. 3, pp. 29-44.

Peterson, J.J., P.J. Fox and E. Schreiber 1974. Newfoundland ophiolites and the geology of the oceanic layer. Nature 247, pp. 194-196.

Raff, A.D. and R.G. Mason 1961. Magnetic survey off the west coast of North America, 40° N to 52° N. Geol. Soc. Amer. Bull. 72, pp. 1267-1270.

Riddihough, R.P. 1977. A model for recent plate interactions off Canada's west coast. Can. J. Earth. Sci. 14, pp 384-396.

Shor, G.G., Jr. 1963. Refraction and reflection techniques and procedure. In: The Sea, M.N. Hill (ed.), Interscience, New York, pp. 20-38.

Srivastava, S.P., D.L. Barrett, C.E. Keen, K.S. Manchester, K.G. Shih, D.L. Tiffin, R.L. Chase, A.G. Thomlinson, E.E. Davis, C.R.B. Lister 1971. Preliminary analysis of geophysical measurements north of Juan de Fuca Ridge. Can. J. Earth Sci. 8, pp. 1265-1280.

Tiffin D.L., B.E.B. Cameron and J.W. Murray 1972. Tectonics and depositional history of the continental margin off Vancouver Island, British Columbia. Can. J. Earth. Sci. 9, pp. 280-296.

_____, 1973. Regional tectonic and sedimentary basin studies on the continental margin off British Columbia. EOS (Amer. Geophys. Union, Trans.), 54, no. 3, pp. 140-141.

_____, and D. Seeman 1975. Bathymetric map of the continental margin of western Canada. Open file map, Geol. Surv. Canada.

Tobin, D.G. and L.R. Sykes 1968. Seismicity and tectonics of the northeast Pacific ocean. J. Geophys. Res. 72, pp. 3821-3846.

Treitel, S., J.L. Shanks and C.W. Frasier 1967. Some aspects of fan filtering. Geophysics 32, pp. 789-800

Wiggins, R.A. 1976. Body wave amplitude calculations-II. Geophys. J. R. astr Soc. 46, pp. 1-10.

_____, and D.V. Helmberger 1974. Synthetic seismogram computation by expansion in generalized rays. Geophys. J. R. astr Soc. 37, pp. 73-90.

_____, and J.A. Madrid 1974. Body wave amplitude calculations. Geophys. J. R. astr. Soc. 37, pp. 423-433.

York, D. 1969. Least squares fitting of a straight line with correlating errors. Earth and Planetary Sci. Lett. 5, pp. 320-324.

FIG. 1.3

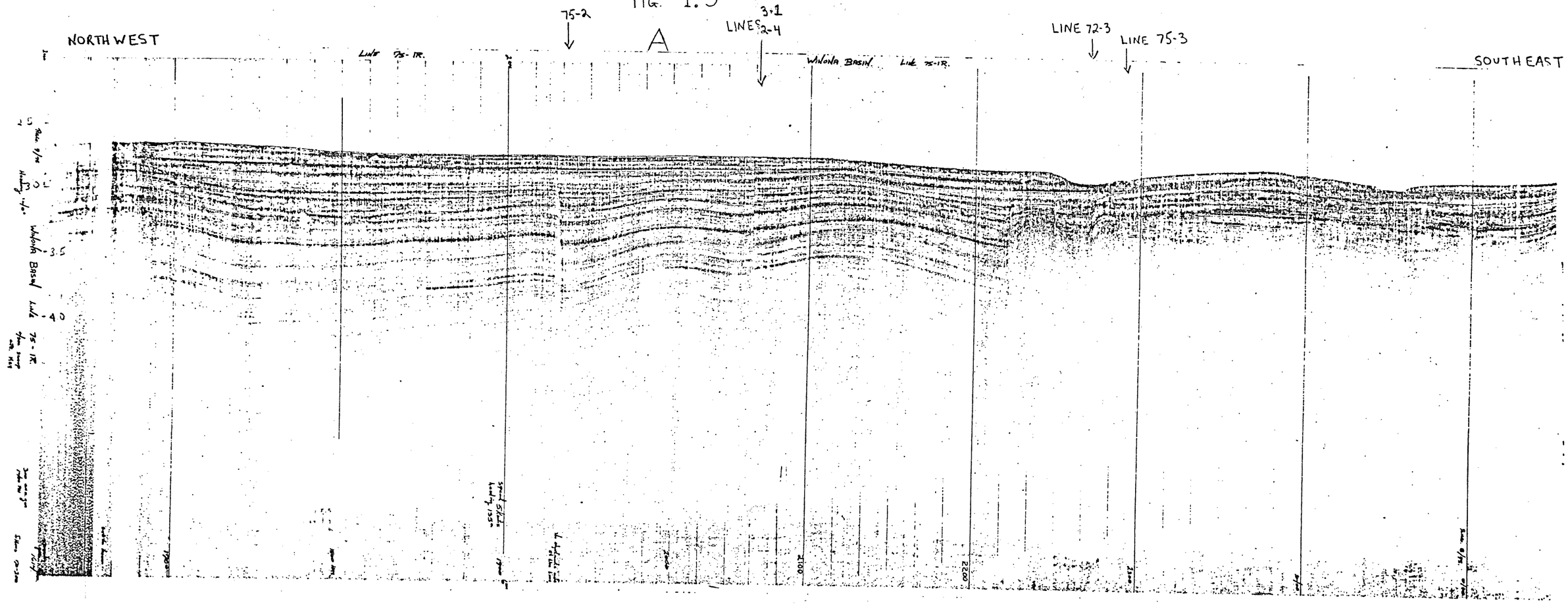
NORTH WEST
A
75-2
LINES 3-1
2-4
LINE 72-3
LINE 75-3
SOUTH EAST
WINONA BASIN
LINE 75-1R.
2100
2200

FIG. 1.3

B

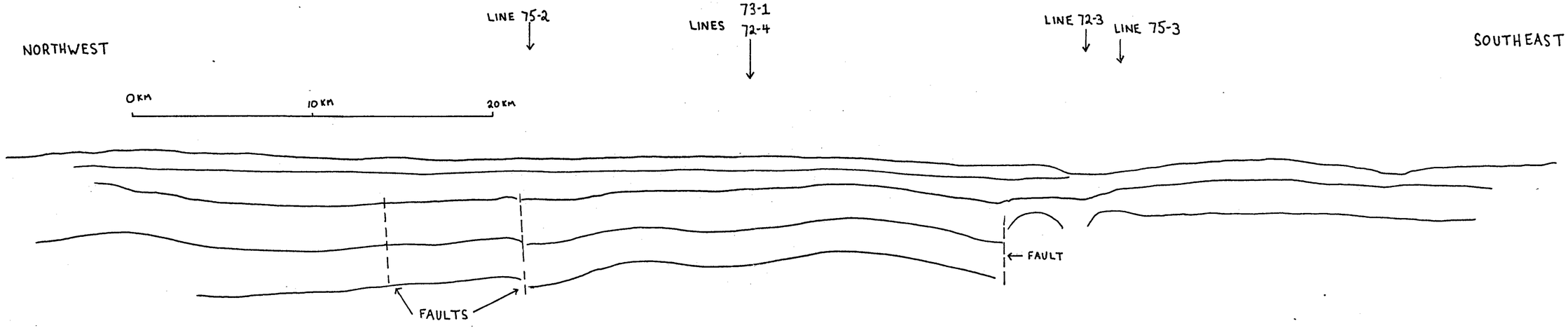
LINE 75-2
LINES 73-1 72-4
LINE 72-3
LINE 75-3
NORTHWEST
SOUTHEAST
0 KM
10 KM
20 KM
FAULT
FAULTS

FIG. 1.4 B

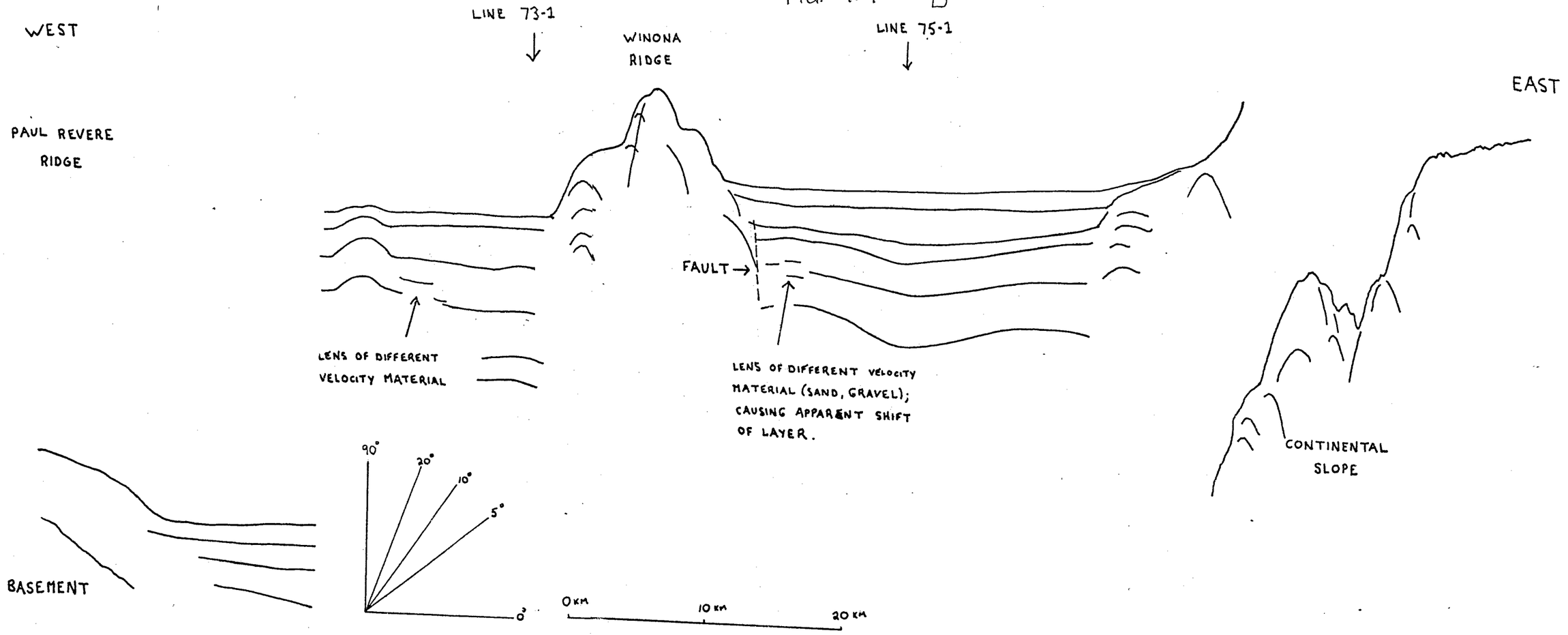
WEST
LINE 73-1
WINONA RIDGE
LINE 75-1
EAST
PAUL REVERE RIDGE
FAULT
LENS OF DIFFERENT VELOCITY MATERIAL
LENS OF DIFFERENT VELOCITY MATERIAL (SAND, GRAVEL); CAUSING APPARENT SHIFT OF LAYER.
CONTINENTAL SLOPE
BASEMENT
90°
20°
10°
5°
0°
0 KM
10 KM
20 KM

FIG. 14 : A

WEST
PAUL REVERE RIDGE
WINONA BASIN
LINE 73-2
LINE 75-2R
WINONA RIDGE
LINE 75-1
WINONA BASIN
75-2R
EAST
END LINE 75-2R